Sanlioglu S, Luleci G, Thomas KW. Simultaneous inhibition of Rac1 and IKK pathways sensitizes lung cancer cells to TNFalpha-mediated apoptosis. Cancer Gene Therapy 2001;8:897–905.
Stefanska J, Pawliczak R. Apocynin: molecular aptitudes. Mediators of Inflammation 2008;2008:106507.
Stolk J, Hiltermann TJ, Dijkman JH, Verhoeven AJ. Characteristics of the inhibition of NADPH oxidase activation in neutrophils by apocynin, a methoxy-substituted catechol. American Journal of Respiratory Cell and Molecular Biology 1994;11:95–102.
Suh J, Rabson AB. NF-kappaB activation in human prostate cancer: important mediator or epiphenomenon? Journal of Cellular Biochemistry 2004;91:100–17.
Suzuki S, Arnold LL, Pennington KL, Kakiuchi-Kiyota S, Cohen SM. Effects of co-administration of dietary sodium arsenite and an NADPH oxidase inhibitor on the rat bladder epithelium. Toxicology 2009;261:41–6.
Ushio-Fukai M. Redox signaling in angiogenesis: role of NADPH oxidase. Cardiovascular Research 2006;71:226–35.
Ushio-Fukai M, Tang Y, Fukai T, Dikalov SI, Ma Y, Fujimoto M, Quinn MT, Pagano PJ, Johnson C, Alexander RW. Novel role of gp91(phox)-containing NAD(P)H oxidase in vascular endothelial growth factor-induced signaling and angiogenesis. Circulation Research 2002;91:1160–7.
Wu WS. The signaling mechanism of ROS in tumor progression. Cancer and Metastasis Reviews 2006;25:695–705.

Cancer Science
The official journal of the Japanese Cancer Association

Apocynin, an NADPH oxidase inhibitor, suppresses rat prostate carcinogenesis

Shugo Suzuki,[1,2,5] Kazuhide Shiraga,[1] Shinya Sato,[1] Wanisa Punfa,[1,3] Aya Naiki-Ito,[1] Yoriko Yamashita,[1] Tomoyuki Shirai[1,4] and Satoru Takahashi[1]

[1]Department of Experimental Pathology and Tumor Biology, Nagoya City University Graduate School of Medical Sciences, Nagoya; [2]Pathology Division, Nagoya City East Medical Center, Nagoya, Japan; [3]Department of Biochemistry, Faculty of Medicine, Chiang Mai University, Chiang Mai, Thailand; [4]Nagoya City Rehabilitation Center, Nagoya, Japan

(Received July 12, 2013/Revised September 6, 2013/Accepted September 19, 2013/Accepted manuscript online September 30, 2013/Article first published online October 28, 2013)

Recent evidence suggests that oxidative stress contributes to the pathogenesis of prostate cancer. The present study focused on the effect of apocynin, an inhibitor of NADPH oxidase, on prostate carcinogenesis using the transgenic rat for adenocarcinoma of prostate (TRAP) model. There were no toxic effects with apocynin treatment. The percentages and numbers of carcinomas in both the ventral and lateral prostate were significantly reduced by apocynin treatment, with dose dependence. Reduction of reactive oxygen species by apocynin was confirmed by immunohistochemistry of 8-OHdG and dihydroethidium staining. Positivity of Ki67 was significantly reduced by apocynin treatment, and downregulation of clusterin expression, as well as inactivation of the MEK-ERK1/2 pathway, was a feature of the apocynin treated groups. In human prostate cancer cell line LNCaP, apocynin also inhibited reactive oxygen species production and blocked cell growth by inducing G0/G1 arrest with downregulation of clusterin and cyclin D1. These data suggest that apocynin possesses chemopreventive potential against prostate cancer. (*Cancer Sci* 2013; 104: 1711–1717)

Prostate cancer is the second most frequently diagnosed cancer in men in the world, with particularly high incidences in Oceania, Europe and North America. In Japan, incident and mortality rates for prostate cancer are relatively low are but increasing.[1,2] There are potentially curative options, such as radical prostatectomy or radiotherapy, but once the disease is metastatic, the outlook is poor. Therefore, research into chemoprevention of prostate cancer is critical.

Reactive oxygen species (ROS) can be important factors for carcinogenesis and tumor progression, not only inducing DNA damage but also producing cellular alterations, such as upregulation of MAPK and protein kinase C.[3,4] Recently, oxidative stress has been reported to contribute to cancer and progression in the prostate.[5,6] Therefore, we have focused on inhibition of ROS production as an anti-carcinogenic approach. ROS is produced by mitochondria, peroxisomes, cytochrome P-450 and other cellular elements as a byproduct, and is generated by NADPH oxidase, which is also implicated in a variety of signaling events, including cell growth, cell survival and cell death.[7] Apocynin, which belongs to the methoxy-substituted catechol family, inhibits NADPH oxidase activity by blocking the formation of NADPH oxidase complex[8] and is commonly used as a standard NOX inhibitor for research purposes.[7] In addition, apocynin can be converted by peroxidase-mediated oxidation to a dimer, which has been shown to be a more efficient inhibitor than apocynin itself.[9] We previously presented evidence that apocynin reduced oxidative stress induced by arsenite treatment of rat urothelium *in vivo*.[10]

In the present study we focus on NADPH oxidase and test whether its inhibitor, apocynin, is able to suppress prostate carcinogenesis in the transgenic rat for adenocarcinoma of prostate (TRAP) model, which was generated in our laboratory and features development of well-differentiated prostate adenocarcinomas in prostatic lobes within a short period. The TRAP rat has a transgene that encodes SV40 T antigen under probasin promoter, so that the carcinomas that develop are androgen-dependent.[11,12]

Materials and Methods

Animal experiment. Male heterozygous TRAP rats established in our laboratory with a Sprague–Dawley genetic background were used in the present study. All animals were housed in plastic cages on wood-chip bedding in an air-conditioned specific pathogen-free animal room at 22 ± 2°C and 55 ± 5% humidity with a 12 h light/dark cycle, and fed a basal diet (Oriental MF, Oriental Yeast, Tokyo, Japan) and provided water, with or without apocynin, *ad libitum*. All animal experiments were performed under protocols approved by the Institutional Animal Care and Use Committee of Nagoya City University School of Medical Sciences.

Six-week-old TRAP rats were divided into three groups of 11 rats each. The animals were given drinking water containing 0, 100 and 500 mg/L apocynin for 8 weeks and body weight and water consumption were estimated every week. At experimental week 8, under deep isoflurane anesthesia, blood was collected from 9.00 to 11.00 h to measure testosterone and estradiol hormone levels using radioimmunoassays from a commercial laboratory (SRL, Tokyo, Japan). Adiponectin concentrations in serum were determined by ELISA (adiponectin ELISA kit; Otsuka Pharmaceutical, Tokyo, Japan). The urogenital complex of each rat was removed as a whole together with the seminal vesicles, then the ventral prostate was weighed. A part of the prostate glands was immediately frozen in liquid nitrogen and stored at −80°C until processed. After that, the remaining tissue was fixed. Livers, kidneys and testes were also removed, weighed and fixed. For clusterin immunostaining, normal prostate glands from a 14-week-old male Sprague–Dawley rat were fixed. The tissues were routinely processed into paraffin-embedded sections and stained with H&E.

Histopathology and immunohistochemistry. Neoplastic lesions in the prostate gland of TRAP rats were evaluated as previously described.[13,14] Briefly, neoplastic lesions were classified into three types: low grade prostatic intraepithelial neoplasia (LG-PIN), high grade PIN (HG-PIN) and adenocarcinoma. The relative numbers of acini with the histological

[5]To whom correspondence should be addressed.
E-mail: shugo@med.nagoya-cu.ac.jp

doi: 10.1111/cas.12292
© 2013 Japanese Cancer Association

characteristics of each type, that is, LG-PIN, HG-PIN and adenocarcinoma, were quantified by counting the total acini in each prostatic lobe. Deparaffinized sections were incubated with diluted antibodies for Ki-67 (Novocastra Laboratories, Newcastle, UK), anti-8-hydroxy-2′-deoxyguanosine (8-OHdG) antibody (Japan Institute for the Control of Aging, Fukuroi, Japan), clusterin (Santa Cruz Biotechnology, Santa Cruz, CA, USA), androgen receptor (AR) and SV40 T antigen (Santa Cruz Biotechnology). The number of Ki-67-labeled or 8-OHdG-labeled cells in at least 1000 cells was counted to determine the labeling indices of HG-PIN and adenocarcinoma.

Detection of reactive oxygen species production. Six-micron frozen serial sections cut on a standard cryostat with clean blades were mounted on slides, then incubated with 5 μM dihydroethidium (Life Technologies, Carlsbad, CA, USA) in PBS for 15 min in the dark. The slides were washed two times with warm PBS and the fluorescence intensity was assessed at 518/605 nm with a spectrofluorometer. Images were also recorded with a fluorescence microscope (BZ-9000; Keyence, Osaka, Japan).

Microarray analysis. Total RNA was isolated from ventral prostate tissues en bloc by phenol–chloroform extraction (ISOGEN, Nippon Gene, Toyama, Japan). Gene expression analysis was performed using a Rat Oligo chip 20k (Toray Industries, Tokyo, Japan) according to the manufacturer's instructions. The RNA ventral prostate expression from 500 mg/L apocynin-treated rats was compared with that from control rats. After global median normalization, data cleansing was performed to remove the values for which fluorescence intensity was <100. The genes for which expression were more than twofold increased or reduced to less than half in 500 mg/L apocynin-treated rats as compared to control rats were selected.

Real-time RT-PCR. Total RNAs from ventral prostate tissues were reverse-transcribed with the ThermoScript first-strand synthesis system (Life Technologies), and real-time RT-PCR was performed using a LightCycler (Roche Diagnostics GmbH, Penzberg, Germany). The quantitative value of clusterin was normalized to endogenous cyclophilin. Clusterin RT-PCR primers were 5′-TTATGGACACAGTGGCAGAG-3′ and 5′-TACAGAACCCAGAGGAAGGA-3′. Cyclophilin RT-PCR primers were 5′-TGCTGGACCAAACACAAATG-3′ and 5′-GAAGGGGAATGAGGAAAATA-3′.

Immunoblot analyses. Ventral prostate tissues were homogenized with RIPA buffer (Pierce Biotechnology, Rockford, IL, USA) containing a protease inhibitor (Pierce Biotechnology) on ice. The insoluble matter was removed by centrifugation at 10 000*g* for 20 min at 4°C and supernatants were collected. Protein concentrations were determined with a Coomassie Plus – The Better Bradford Assay Kit (Pierce Biotechnology). Samples were mixed with 2× sample buffer (Bio-Rad Laboratories, Hercules, CA, USA) and heated for 5 min at 95°C and then subjected to SDS-PAGE. The separated proteins were transferred onto nitrocellulose membranes followed by blocking with SuperBlock Blocking Buffer (Thermo Fisher Scientific, Waltham, MA, USA) for 1 h at room temperature. Membranes were probed with antibodies for cyclin D1, clusterin, cleaved caspase-3, MEK, phospho-MEK, p44/42 MAPK (ERK1/2), phopho-ERK1/2, p38 MAPK, phospho-p38 MAPK, and caspase 3 and 7 (Cell Signaling Technology, Danvers, MA, USA) in 1× TBS with 0.1% Tween 20 at 4°C overnight, followed by exposure to peroxidase-conjugated appropriate secondary antibodies and visualization with an enhanced chemiluminescence detection system (GE Healthcare Bio-sciences, Buckinghamshire, NA, UK). To confirm equal protein loading, each membrane was stripped and reprobed with anti-β-actin (Sigma-Aldrich, St. Louis, MO, USA).

Cell line. The human androgen-dependent prostate cancer cell line LNCaP was obtained from the American Type Culture Collection (Manassas, VA, USA). The cells were grown in RPMI1640 medium with 10% FBS, 100 U/mL penicillin and 100 μg/mL streptomycin (all from Life Technologies) under an atmosphere of 95% air and 5% CO_2 at 37°C.

Cell proliferation assay. Cell proliferation of prostate cancer cell lines was assessed by 4-[3-(4-iodophenyl)-2-(4-nitrophenyl)-2H-5-tetrazolio]-1,3-benzene disulfonate tetrazolium salt (WST-1) assay (Roche Applied Science, Mannheim, Germany). Briefly, cells were seeded in 96-well plates at 500 cells/well in 200 μL of culture medium. Apocynin was added 24 h after seeding and incubated for 3 days. WST-1 reagent was added to each well with incubation for 60 min at 37°C, and then each well was measured for absorbance at 430 nm.

Detection of reactive oxygen species production in LNCaP cells. The culture supernatant was removed from all wells 24 h after apocynin treatment, and the cells were washed twice with warm PBS, then 2′,7′-dichlorofluorescin-diacetate (100 μg/mL, DCFH-DA, Sigma-Aldrich) was added with further incubation at 37°C for 20 min, in the dark. The cells were washed two times with warm RPMI1640 medium, and images were recorded using a fluorescence microscope (BZ-9000; Keyence).

Cell cycle analysis. Cells were treated with apocynin for 24 h, then suspensions were prepared and stained with propidium iodide (Guava Cell Cycle Reagent, Guava Technologies, Hayward, CA, USA) according to the Guava Cell Cycle Assay protocol. Cell cycle phase distributions were determined on a Guava PCA Instrument using CytoSoft Software.

Statistical analysis. All *in vitro* experiments were performed at least in triplicate to confirm reproducibility. Statistical analyses were performed with mean ± SD values using one-way ANOVA and Dunnett's test. Statistical significance was concluded at $*P < 0.05$, $**P < 0.01$ or $***P < 0.001$.

Results

Apocynin reduction of progression of prostate tumorigenesis as well as cell proliferation and reactive oxygen species in TRAP rats. During the experiments, water consumption by 500 mg/L apocynin-treated rats was approximately 10% lower than in the controls (Table 1). However, administration of apocynin did not cause adverse effects (e.g. impacting the growth of rats) during the study. There were no significant differences in the final body weights or in absolute and relative liver,

Table 1. Body and organ weights, water consumption

Treatment	Number of rats	Body weight (g)	Liver (g)	Kidneys (g)	Testes (g)	Ventral prostate (g)	Water consumption (mL/rat/day)
Control	11	533 ± 58	18.5 ± 2.0	3.2 ± 0.2	3.5 ± 0.4	0.30 ± 0.06	45.5 ± 4.4
100 mg/L	11	553 ± 49	20.1 ± 2.3	3.1 ± 0.3	3.6 ± 0.3	0.36 ± 0.09	46.5 ± 5.5
500 mg/L	11	558 ± 65	20.2 ± 3.2	3.2 ± 0.4	3.6 ± 0.4	0.30 ± 0.04	39.6 ± 2.6*

*Significantly different from control group, $P < 0.05$.

doi: 10.1111/cas.12292
© 2013 Japanese Cancer Association

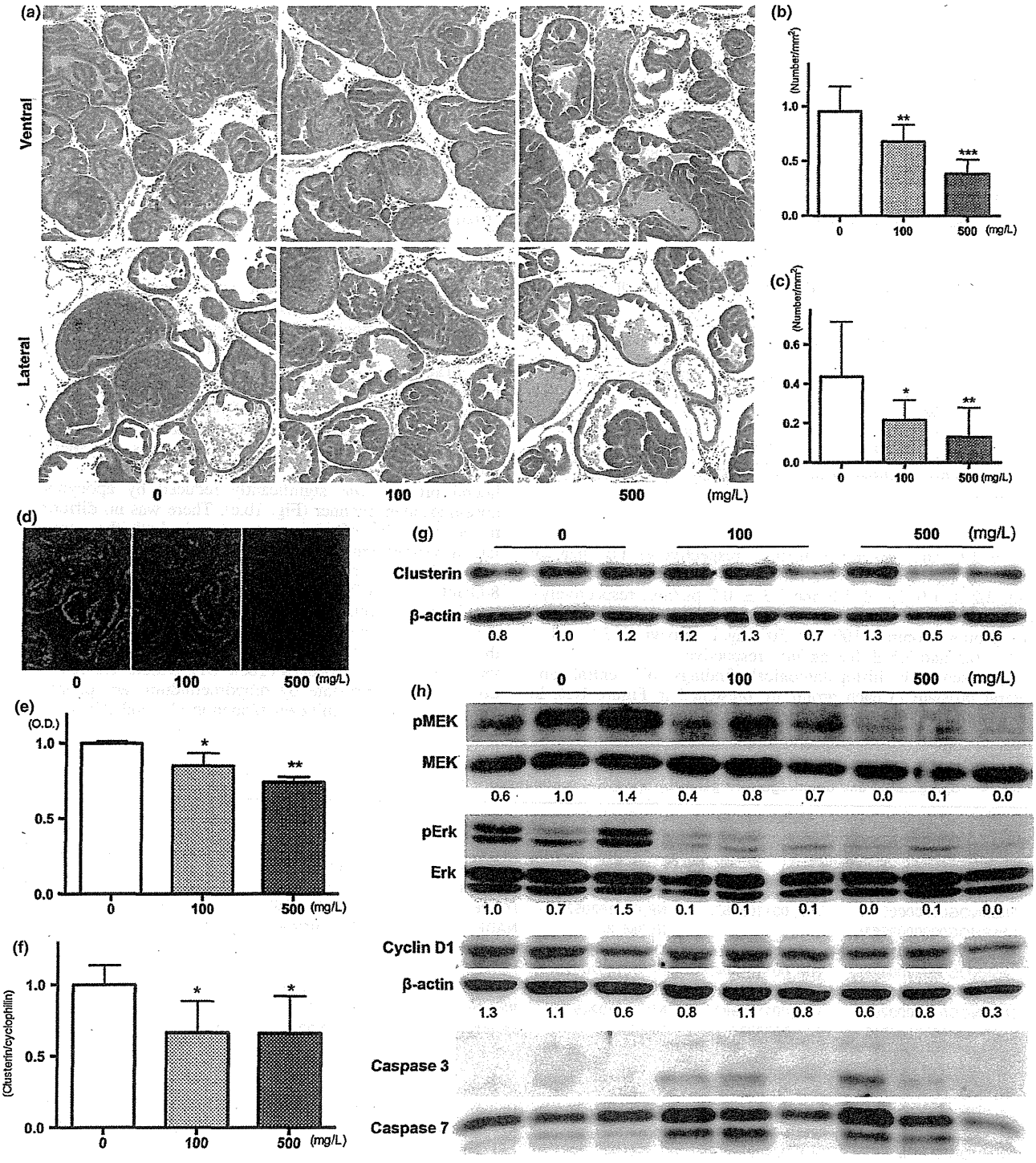

Fig. 1. Effects of apocynin on prostatic lesions. Representative histopathological findings for lesions in the ventral and lateral prostates of the controls, 100 and 500 mg/L apocynin groups (a). Number of adenocarcinoma per area in ventral (b) and lateral (c) prostate of TRAP rats treated with apocynin. Photos (d) and data (e) for reactive oxygen species production detected by dihydroethidium staining in ventral prostate of TRAP rats treated with apocynin. Expression of clusterin detected by quantitative RT-PCR (f) and western blotting (g). Results of immunoblot analysis of MAPK, cyclin D1 and caspases in ventral prostates of TRAP rats treated with apocynin. Data are mean ± SD values from 3 independent experiments. *,**,***$P < 0.05$, 0.01 and 0.001 compared to controls, respectively.

kidney, testes and prostate weights among the groups (Table 1). Histologically, there were no changes indicative of toxicity in the liver, kidneys, and testes with apocynin (data not shown). The serum level of testosterone in 500 mg/L apocynin treated rats (3.1 ± 1.6 ng/mL) was slightly higher than in other groups (control and 100 mg/L apocynin:

© 2013 Japanese Cancer Association

Table 2. Incidence of carcinoma and quantitative evaluation of neoplastic lesions in ventral and lateral prostate

Treatment	Number of rats	Ventral				Lateral			
		Incidence of carcinoma	% of lesions in prostate			Incidence of carcinoma	% of lesions in prostate		
			LG-PIN	HG-PIN	Carcinoma		LG-PIN	HG-PIN	Carcinoma
Control	11	11 (100%)	6.6 ± 2.5	81.8 ± 4.8	11.7 ± 4.5	10 (91%)	11.8 ± 5.2	82.8 ± 6.8	5.4 ± 3.9
100 mg/L	11	11 (100%)	8.0 ± 2.5	83.6 ± 3.8	8.4 ± 2.8*	10 (91%)	17.4 ± 4.3	80.1 ± 4.3	2.5 ± 1.4*
500 mg/L	11	11 (100%)	8.3 ± 1.6	87.3 ± 3.2**	4.4 ± 1.9***	6 (55%)	26.8 ± 9.9***	71.8 ± 9.0**	1.5 ± 1.7**

*,**,***Indicate significant difference from the control group, $P < 0.05$, 0.1, 0.001, respectively.

Table 3. Labeling indices of Ki67 and 8-OHdG in HG-PIN of ventral and lateral prostate

Treatment	Ventral prostate		Lateral prostate	
	Ki67	8-OHdG	Ki67	8-OHdG
Control	52.6 ± 1.1	2.9 ± 0.4	49.7 ± 1.6	2.7 ± 0.4
100 mg/L	43.8 ± 2.2***	2.3 ± 0.4**	35.2 ± 7.2***	2.0 ± 0.2***
500 mg/L	24.4 ± 1.8***	1.5 ± 0.3***	18.4 ± 2.8***	1.5 ± 0.2***

**, ***Significantly different from control group, $P < 0.01$, 0.001, respectively.

1.7 ± 1.0 and 1.9 ± 0.8 ng/mL, respectively) but that of estradiol was not affected (control, 100 and 500 mg/L apocynin: 3.2 ± 1.0, 3.4 ± 1.2 and 3.3 ± 0.7 pg/mL, respectively). Adiponection concentration in the serum did not differ among the groups (control, 100 and 500 mg/L apocynin: 3.5 ± 1.1, 3.2 ± 0.5 and 3.5 ± 0.8 ng/mL, respectively).

Representative histopathological findings of ventral and lateral prostate in each group are presented in Figure 1(a). In the ventral prostate, there was a marked or partial pathologic response to apocynin treatment, as demonstrated by a significant reduction in the prostatic neoplastic lesions in TRAP rats; however, small foci of PIN remained. Decrease in the incidence of adenocarcinoma was also observed in the lateral prostate (Table 2). Quantitative evaluation of the proportion of preneoplastic and neoplastic lesions in the prostate gland showed significant suppression of progression from LG-PIN or HG-PIN to adenocarcinoma in rats treated with apocynin in a dose-dependent manner (Table 2). To focus on adenocarcinoma, the number of foci per area in both the ventral and lateral prostate was significantly reduced by apocynin in a dose-dependent manner (Fig. 1b,c). There was no difference in the average size of adenocarcinomas in both the ventral and lateral prostate among the groups (data not shown). There was a significant decrease in the labeling index of Ki-67 and 8-OHdG in HG-PIN of the ventral and lateral prostates of TRAP rats given apocynin in a dose-dependent manner (Table 3). Although the rate of significance was slightly less, the results were mostly the same in the adenocarcinoma of the ventral and lateral prostates (Table S1). Results for ROS detection in ventral prostate by dihydroethidium are presented in Figure 1(d), with significant reduction (11 and 22% reduction

Table 4. Upregulated and downregulated genes by apocynin treatment in ventral prostate

ID	Reference ID	Symbol	Description	Ratio
Upregulated genes				
ENSRNOG00000038093	–	LAC2_RAT	Ig lambda-2 chain C region	5.62
ENSRNOG00000033745	–	Q5FVP9_RAT	Cfh protein	3.10
ENSRNOG00000005743	NM_001108582.1	NP_001102052.1	LOC362136 (predicted) (RGD1309610_predicted), mRNA	2.58
ENSRNOG00000033615	–	NU3M_RAT	NADH-ubiquinone oxidoreductase chain 3 (EC 1.6.5.3)	2.45
ENSRNOG00000015155	NM_001037351.1	Tnnc2	Troponin C2, fast	2.11
ENSRNOG00000008746	NM_001108594.1	NP_001102064.1	Histidyl tRNA synthetase 2	2.07
ENSRNOG00000001333	NM_012826.1	Azgp1	Zinc-alpha-2-glycoprotein precursor	2.06
ENSRNOG00000002871	NM_001108984.1	NP_001102454.1	RNA binding motif protein 25	2.05
ENSRNOG00000023151	NM_203333.2	Scgb2a2	Secretoglobin family 2A member 2 precursor	2.01
Downregulated genes				
ENSRNOG00000021604	NM_001008835.1	RT1-CE1	RT1 class I, CE1	0.28
ENSRNOG00000002343	NM_017237.2	Uchl1	Ubiquitin carboxyl-terminal hydrolase isozyme L1 (EC 3.4.19.12)	0.36
ENSRNOG00000038999	NM_001008827.1	RT1-A1	RT1 class Ia, locus A1	0.36
ENSRNOG00000029579	NM_001008840.1	RT1-CE2	RT1 class I, CE2	0.41
ENSRNOG00000030251	–	RT1-CE10	RT1 class I, CE10	0.41
ENSRNOG00000032872	–	UBIQ_RAT	Ubiquitin	0.43
ENSRNOG00000034234	–	COX1_RAT	Cytochrome c oxidase subunit 1 (EC 1.9.3.1)	0.43
ENSRNOG00000037414	–	Q5I1B4_RAT	ABP beta (Fragment)	0.44
ENSRNOG00000030371	–	COX2_RAT	Cytochrome c oxidase subunit 2	0.45
ENSRNOG00000039668	NM_001107100.1	NP_001100570.1	Procollagen, type VIII, alpha 1	0.46
ENSRNOG00000016460	NM_053021.2	Clu	Clusterin precursor	0.49
ENSRNOG00000011647	NM_053485.2	S100a6	Protein S100-A6	0.50
ENSRNOG00000007539	NM_138881.1	Best5	Radical S-adenosyl methionine domain-containing protein 2	0.50
ENSRNOG00000002052	NM_022543.2	Ssg1	Coiled-coil domain-containing protein 80 precursor	0.50

doi: 10.1111/cas.12292
© 2013 Japanese Cancer Association

at 100 and 500 mg/L, respectively) documented (Fig. 1e). Androgen receptors and SV40 T antigen were diffusely detected immunohistochemically in areas of PIN and adenocarcinomas in the ventral and lateral prostate, with no differences among the groups (data not shown).

Reduction of cell proliferation by apocynin treatment was associated with changes in clusterin and the MEK-ERK1/2 pathway. To elucidate the mechanisms of anti-carcinogenesis of apocynin, microarray analysis was performed (GEO: GSE47200). Genes that were upregulated or downregulated by apocynin are listed in Table 4. After selection, 9 upregulated and 14 downregulated genes were detected, some related to oxidative responses (NADH-ubiquinone oxidoreductase chain 3, cytochrome c oxidase subunit 1 and 2) and others immunological responses (Ig lambda-2 chain C region, Cfh protein, secretoglobin family 2A member 2 precursor, RT1 class I, CE1, CE2 and CE10, RT1 class Ia, locus A1). Because apocynin reduced rat prostate carcinogenesis, we focused on the clusterin precursor belonging to downregulated genes, which is known to be related to tumorigenesis in many sites. Reduction of clusterin expression in the ventral prostate of apocynin-treated rats was confirmed by real-time RT-PCR (Fig. 1f) and also by western blotting (Fig. 1g). Immunohistochemical analyses revealed that clusterin expression was observed mainly in the epithelial membranes of the ventral prostate of TRAP rats, but no staining was observed in the epithelium of the prostate of Sprague–Dawley rats (Fig. S1a). Differences in the intensity of clusterin immunostaining determined by optical density measurement was relatively inconspicuous among LG-PIN, HG-PIN or adenocarcinoma in the ventral lobes of the control TRAP rats (Fig. S1b). However, clusterin expression in HG-PIN of ventral prostate of apocynin-treated TRAP rats was significantly reduced compared to the control (Fig. S1c; control, 100 and 500 mg/L apocynin: 50.1 ± 5.0, 43.2 ± 7.4 and 35.6 ± 4.3, respectively). Reduction of phosphorylation in MEK and p44/42 MAPK (ERK1/2), and cyclin D1 were also detected. Cleaved caspases 3 and 7 were detected in the ventral prostate of some apocynin-treated rats (Fig. 1h).

Apocynin affected reduction of cell growth via the same pathways in a human prostate cancer cell line. In the human prostate cell line, significant reduction of cell growth and ROS generation was detected after apocynin treatment at concentrations higher than 250 μM (Fig. 2a,b). Apocynin-treated cells appeared to accumulate in G1 phase at 500 μM, compared to the controls ($P < 0.05$), with concomitant decrease in the percentage of cells in the S phase (Fig. 2c). Downregulation of clusterin around 70 kDa and cyclin D1 expression were detected by western blotting (Fig. 2d).

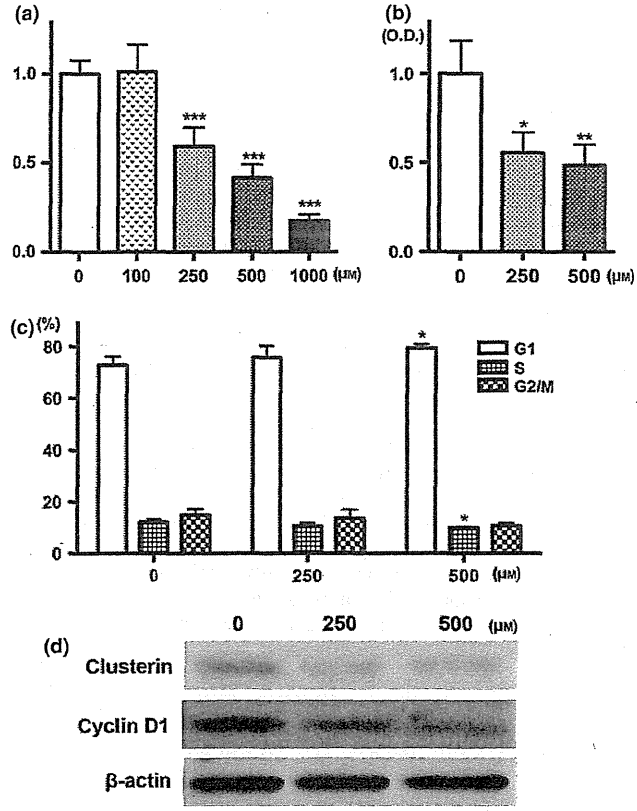

Fig. 2. Anti-growth effects of apocynin in LNCaP cells. Cells were incubated with apocynin for 72 h and then cytotoxicity was assessed by WST-1 assay (a). Reactive oxygen species production data detected by DCFH-DA after apocynin treatment for 24 h (b). Cell cycle distribution of LNCaP cells after treatment with apocynin for 24 h (c). Immunoblot analysis of the protein levels of clusterin, cyclin D1 and ß-actin with apocynin treatment (d). $*P < 0.05$, $**P < 0.01$ and $***P < 0.001$ compared to controls. O.D, optical density.

Discussion

In the present study, we demonstrated suppressive effects of apocynin treatment on prostatic carcinogenesis in the TRAP rat model. Because apocynin is known to be an NADPH oxidase inhibitor, we focused on ROS conditions in prostate tissue using immunohistochemistry for 8-OHdG and dihydroethidium staining. Some reports have indicated that antioxidants such as N-acetylcysteine and vitamin C clearly reduce oxidative stress *in vitro*, but exert less effects with oral dosing *in vivo*.[15,16] ROS is generally produced from mitochondria, peroxisomes, cytochrome P450 and NADPH oxidase.[4,6,7] Apocynin only affects ROS reduction from NADPH oxidase, but it would be expected to be a good antioxidant *in vivo*. In addition, we did not detect any toxic effects of apocynin in this study.

Reactive oxygen species generation is not only considered associated with tissue injury and/or DNA damage, but also neoplastic transformation, aberrant growth and/or proliferation.[4,7] Indeed, ROS may play broad roles in cellular processes associated with initiation and development of many cancers, including prostate cancer.[6] In this study, apocynin reduced the Ki-67 labeling index and cyclin D1 expression, which indicates that ROS generation is related to cell proliferation in prostate lobes of TRAP rats. Furthermore, NADPH oxidase is reported to regulate plasma adiponectin,[17] whose concentration may be negatively correlated with prostate cancer progression.[18] Therefore, we investigated adiponectin concentration in serum, but did not find any differences among the groups.

In TRAP rats, we previously detected activation of p38 MAPK and ERK1/2 in prostate tissue, and inactivation by chemopreventive agents such as angiotensin II receptor blocker or purple corn color.[14,19] These also reduced cell proliferation and/or induced apoptosis in prostate tissue. In this study, we also detected dephosphorylation of ERK1/2 in the prostate after apocynin treatment. To assess the relationship between ROS generation and phosphorylation of ERK1/2, microarray analysis was employed. The data obtained for upregulated and downregulated genes indicated associations with ROS generation, immune function and translation by gene ontology.[20] We focused on clusterin, dysregulated in many types of cancer, including prostate cancer,[21] with cellular functions such as a sulfated glycoprotein in regulation of apoptosis, cell cycle control, DNA repair, cell adhesion and tissue remodeling.[22,23] It has two isoforms. Secretory clusterin (sCLU) has a chaperone

© 2013 Japanese Cancer Association

action like that of small heat shock proteins, and is sized around 70–80 kDa. The other clusterin isoform is the nuclear form (nCLU) of 55 kDa, associated with cell death.[21–23] In this study, we detected significant reduction of clusterin protein around 70 kDa. Because sCLU is reported to be downregulated by p53 in some tumor cells,[22] high expression of clusterin in the prostate would be expected given dysfunction of p53 under the influence of SV40 T antigen in TRAP rats.[24]

In human prostate cancer, clusterin expression is initially low in contrast with the prostate cancer cells resistant to conventional chemotherapy or hormonal therapy which show upregulation.[21,25] Meanwhile, we detected rather high expression of clusterin in all stages of prostate cancer development in TRAP rats. In te transgenic adenocarcinoma of mouse prostate (TRAMP) model, higher expression of clusterin in the prostate glands was detected compared to that in non-transgenic mice; however, analyses of overt carcinoma revealed no expression.[26] These data suggest that SV40 T antigen supports to induce clusterin expression among the carcinogenic process in the prostate of both mice and rats. The difference in clusterin expression in carcinoma may be related to the different histology between mice (poorly-differentiated neuroendocrine-like carcinomas) and rats (moderately differentiated adenocarcinomas), because clusterin is mainly stained in the membrane.

Recently, sCLU was reported to induce phosphorylation of ERK1/2 in lung adenocarcinoma and pancreatic cancer cells.[27,28] Therefore, we considered that apocynin reduced prostate carcinogenesis via clusterin, acting on the ERK1/2 pathway and reducing cell proliferation in TRAP rats. We also found that apocynin reduced cell growth and ROS generation, along with expression of clusterin and cyclin D1 in LNCaP cells (human prostate cell line). Although there is a possibility that the exact intracellular molecular pathways affected by apocynin treatment may be different between humans and rats, we suggest that there may be similar anti-neoplastic effects caused by apocynin, especially related to clusterin expression, in rat and human prostate.

Chemoprevention attempts are comprehensive in prostate cancer, and various agents are reported to prevent, reverse or delay tumor deveolpment and progression.[29] In this study, we detected lower incidence of adenocarcinoma in the lateral lobes of 500 mg/L apocynin-treated rats, and reduction of cell proliferation was observed in both PIN and adenocarcinoma. Thus, we consider that apocynin has potential to prevent and delay the carcinogenic process, and is suitable as a chemopreventive drug. Recently, custirsen (OGX-011), a clusterin inhibitor, was selected for use as an anti-cancer drug in a randomized phase II study of patients with metastatic castration-resistant prostate cancer.[30,31] We earlier reported that apocynin inhibited growth of androgen-independent prostate cancer with inhibition of phosphorylation of Rac1 and NF-κB and angiogenesis.[32] Together with the present data, we confirm that apocynin has the potential to be a candidate anti-cancer drug for androgen-dependent/independent prostate cancer.

In conclusion, apocynin, an NADPH oxidase inhibitor, suppressed prostate carcinogenesis while reducing ROS in the TRAP rat model. The mechanism of prevention appears to involve regulation of cell proliferation via clusterin and the MEK-ERK1/2 pathway. Apocynin warrants further attention as a promising chemopreventive drug for prostate cancer.

Acknowledgments

This work was supported by a Grant-in-Aid for the 3rd Term Comprehensive 10-Year Strategy for Cancer Control from the Ministry of Health, Labour and Welfare of Japan and grants from Ono Pharmaceutical, the Society for Promotion of Pathology in Nagoya, and the Research Foundation for Oriental Medicine. The authors would like to thank Dr Malcolm Moore for his help in reviewing this manuscript.

Disclosure Statement

The authors have no conflict of interest.

References

1 Jemal A, Bray F, Center MM, Ferlay J, Ward E, Forman D. Global cancer statistics. *CA Cancer J Clin* 2011; **61**: 69–90.
2 Damber JE, Aus G. Prostate cancer. *Lancet* 2008; **371**: 1710–21.
3 Lee YJ, Lee JH, Han HJ. Extracellular adenosine triphosphate protects oxidative stress-induced increase of p21(WAF1/Cip1) and p27(Kip1) expression in primary cultured renal proximal tubule cells: role of PI3K and Akt signaling. *J Cell Physiol* 2006; **209**: 802–10.
4 Wu WS. The signaling mechanism of ROS in tumor progression. *Cancer Metastasis Rev* 2006; **25**: 695–705.
5 Kumar B, Koul S, Khandrika L, Meacham RB, Koul HK. Oxidative stress is inherent in prostate cancer cells and is required for aggressive phenotype. *Cancer Res* 2008; **68**: 1777–85.
6 Khandrika L, Kumar B, Koul S, Maroni P, Koul HK. Oxidative stress in prostate cancer. *Cancer Lett* 2009; **282**: 125–36.
7 Bedard K, Krause KH. The NOX family of ROS-generating NADPH oxidases: physiology and pathophysiology. *Physiol Rev* 2007; **87**: 245–313.
8 Stolk J, Hiltermann TJ, Dijkman JH, Verhoeven AJ. Characteristics of the inhibition of NADPH oxidase activation in neutrophils by apocynin, a methoxy-substituted catechol. *Am J Respir Cell Mol Biol* 1994; **11**: 95–102.
9 Stefanska J, Pawliczak R. Apocynin: molecular aptitudes. *Mediators Inflamm* 2008; **2008**: 106507.
10 Suzuki S, Arnold LL, Pennington KL, Kakiuchi-Kiyota S, Cohen SM. Effects of co-administration of dietary sodium arsenite and an NADPH oxidase inhibitor on the rat bladder epithelium. *Toxicology* 2009; **261**: 41–6.
11 Asamoto M, Hokaiwado N, Cho YM *et al.* Prostate carcinomas developing in transgenic rats with SV40 T antigen expression under probasin promoter control are strictly androgen dependent. *Cancer Res* 2001; **61**: 4693–700.
12 Cho YM, Takahashi S, Asamoto M *et al.* Age-dependent histopathological findings in the prostate of probasin/SV40 T antigen transgenic rats: lack of influence of carcinogen or testosterone treatment. *Cancer Sci* 2003; **94**: 153–7.
13 Seeni A, Takahashi S, Takeshita K *et al.* Suppression of prostate cancer growth by resveratrol in the transgenic rat for adenocarcinoma of prostate (TRAP) model. *Asian Pac J Cancer Prev* 2008; **9**: 7–14.
14 Long N, Suzuki S, Sato S *et al.* Purple corn color inhibition of prostate carcinogenesis by targeting cell growth pathways. *Cancer Sci* 2013; **104**: 298–303.
15 Wang Z, Zhou J, Lu X, Gong Z, Le XC. Arsenic speciation in urine from acute promyelocytic leukemia patients undergoing arsenic trioxide treatment. *Chem Res Toxicol* 2004; **17**: 95–103.
16 Gibson KR, Neilson IL, Barrett F *et al.* Evaluation of the antioxidant properties of N-acetylcysteine in human platelets: prerequisite for bioconversion to glutathione for antioxidant and antiplatelet activity. *J Cardiovasc Pharmacol* 2009; **54**: 319–26.
17 Furukawa S, Fujita T, Shimabukuro M *et al.* Increased oxidative stress in obesity and its impact on metabolic syndrome. *J Clin Invest* 2004; **114**: 1752–61.
18 Goktas S, Yilmaz MI, Caglar K, Sonmez A, Kilic S, Bedir S. Prostate cancer and adiponectin. *Urology* 2005; **65**: 1168–72.
19 Takahashi S, Uemura H, Seeni A *et al.* Therapeutic targeting of angiotensin II receptor type 1 to regulate androgen receptor in prostate cancer. *Prostate* 2012; **72**: 1559–72.
20 Ashburner M, Ball CA, Blake JA *et al.* Gene ontology: tool for the unification of biology. The Gene Ontology Consortium. *Nat Genet* 2000; **25**: 25–9.
21 Rizzi F, Bettuzzi S. The clusterin paradigm in prostate and breast carcinogenesis. *Endocr Relat Cancer* 2010; **17**: R1–17.
22 Shannan B, Seifert M, Leskov K *et al.* Challenge and promise: roles for clusterin in pathogenesis, progression and therapy of cancer. *Cell Death Differ* 2006; **13**: 12–9.
23 Shannan B, Seifert M, Boothman DA, Tilgen W, Reichrath J. Clusterin and DNA repair: a new function in cancer for a key player in apoptosis and cell cycle control. *J Mol Histol* 2006; **37**: 183–8.

doi: 10.1111/cas.12292
© 2013 Japanese Cancer Association

24 Ahuja D, Saenz-Robles MT, Pipas JM. SV40 large T antigen targets multiple cellular pathways to elicit cellular transformation. *Oncogene* 2005; **24**: 7729–45.
25 Rizzi F, Bettuzzi S. Clusterin (CLU) and prostate cancer. *Adv Cancer Res* 2009; **105**: 1–19.
26 Caporali A, Davalli P, Astancolle S *et al.* The chemopreventive action of catechins in the TRAMP mouse model of prostate carcinogenesis is accompanied by clusterin over-expression. *Carcinogenesis* 2004; **25**: 2217–24.
27 Chou TY, Chen WC, Lee AC, Hung SM, Shih NY, Chen MY. Clusterin silencing in human lung adenocarcinoma cells induces a mesenchymal-to-epithelial transition through modulating the ERK/Slug pathway. *Cell Signal* 2009; **21**: 704–11.
28 Tang Y, Liu F, Zheng C, Sun S, Jiang Y. Knockdown of clusterin sensitizes pancreatic cancer cells to gemcitabine chemotherapy by ERK1/2 inactivation. *J Exp Clin Cancer Res* 2012; **31**: 73.
29 Gupta S. Prostate cancer chemoprevention: current status and future prospects. *Toxicol Appl Pharmacol* 2007; **224**: 369–76.
30 Saad F, Hotte S, North S *et al.* Randomized phase II trial of Custirsen (OGX-011) in combination with docetaxel or mitoxantrone as second-line therapy in patients with metastatic castrate-resistant prostate cancer progressing after first-line docetaxel: CUOG trial P-06c. *Clin Cancer Res* 2011; **17**: 5765–73.
31 Chi KN, Hotte SJ, Yu EY *et al.* Randomized phase II study of docetaxel and prednisone with or without OGX-011 in patients with metastatic castration-resistant prostate cancer. *J Clin Oncol* 2010; **28**: 4247–54.
32 Suzuki S, Pitchakarn P, Sato S, Shirai T, Takahashi S. Apocynin, an NADPH oxidase inhibitor, suppresses progression of prostate cancer via Rac1 dephosphorylation. *Exp Toxicol Pathol* 2013; **65**: 1035–41.

Supporting Information

Additional supporting information may be found in the online version of this article:

Fig. S1. Expression of clusterin in ventral lobe of prostate. Pictures of H&E and immunohistochemistry of clusterin in normal epithelium in Sprague–Dawley rat, LG-PIN, HG-PIN and carcinoma in TRAP rats (a) and expression of clusterin (b). Expression of clusterin in HG-PIN of ventral lobe of control, 100 and 500 mg/L apocynin treated rats (c). Carcinoma; Adenocarcinoma. *,***$P < 0.05$ and 0.001 compared to Normal epithelium or control, respectively.

Table S1. Labeling indices of Ki67 and 8-OHdG in adenocarcinoma of ventral and lateral prostate.

© 2013 Japanese Cancer Association

*J Toxicol Pathol 2014; 27: **–****

Original Article

Establishment of an Invasive Prostate Cancer Model in Transgenic Rats by Intermittent Testosterone Administration

Shinya Sato[1], Shugo Suzuki[1], Aya Naiki-Ito[1], Masami Komiya[1, #], Long Ne[1, ##], Hiroyuki Kato[1], Hiroyuki Sagawa[1], Yoriko Yamashita[1], Tomoyuki Shirai[1, ###], and Satoru Takahashi[1]

[1] Department of Experimental Pathology and Tumor Biology, Nagoya City University Graduate School of Medical Sciences, 1 Kawasumi, Mizuho-cho, Mizuho-ku, Nagoya 467-8601, Japan

Abstract: We have established a transgenic rat for adenocarcinoma of the prostate (TRAP) model that features uniform adenocarcinoma development in prostatic lobes at high incidence within a short experimental period. However, no invasive carcinomas with reactive stroma characteristics similar to those in man were observed. We therefore have focused on a new model for invasive carcinoma of the prostate using TRAP rats. In experiment 1, male TRAP rats in groups 1 and 2 were treated with orchiectomy at day 0 of the experiment. Rats in groups 1–3 underwent testosterone propionate (TP) implantation from weeks 1 to 4 and from weeks 6 to 16. Rats in groups 1 and 3 were given 3,2'-dimethyl-4-aminobiphenyl (DMAB) after TP implantation. The rats of group 4 served as controls. In experiment 2, the rats were divided into three groups, none of which received DMAB or orchiectomy, treated with TP continuously or with the treatment withdrawn once or twice. In experiment 1, invasive adenocarcinomas with abundant collagenous stroma were found in the dorsolateral and anterior prostate, some of which showed perineural space invasion at week 16. The number of invasive carcinoma foci was most frequent in group 3. In experiment 2, invasive adenocarcinoma development in the lateral prostates was correlated with the number of TP administration/withdrawal cycles. In conclusion, our newly established rat model for invasive adenocarcinoma of the prostate could serve as a useful preclinical model for evaluating the *in vivo* efficacy of preventive and therapeutic agents targeting of the tumor microenvironment. (DOI: 10.1293/tox.27.**; J Toxicol Pathol 2014; 27: **–**)

Key words: prostate cancer, animal model, cancer invasion, transgenic rat, testosterone propionate, intermittent administration

Introduction

Prostate cancer is the most common cancer and the second leading cause of death from cancer among men in the US. It has been estimated there will be approximately 238,590 new cases of prostate cancer and 29,720 deaths from prostate cancer in the US in 2013[1]. In Japan, the prevalence and mortality of prostate cancer has also been increasing, along with in the so-called nutrition transition[2, 3]. Androgen ablation therapy is generally applied for prostate cancer because of hormone-dependent growth. However, outgrowth of androgen-independent and metastatic cancer cells is a frequent outcome, eventually leading to death of the patient. Therefore, understanding of the mechanisms of the acquisition of metastatic potential or the androgen-independent phenotype of cancer cells is urgently required.

We have established a rat cancer model responding to the need for *in vivo* systems that adequately reproduce the spectrum of human prostate cancers. Administration of 3,2'-dimethyl-4-aminobiphenyl (DMAB) induces noninvasive and androgen-dependent adenocarcinomas in the ventral prostate, while additional long-term treatment with testosterone propionate (TP) causes development of invasive and metastasizing androgen-independent adenocarcinomas arising from the dorsolateral and anterior prostate and seminal vesicles[4, 5]. However, a long period of about 60 weeks is required to induce prostate cancers in both carcinogenesis models, and the incidence of lesion development is relatively low. Therefore, we have established transgenic rats bearing a probasin promoter/simian virus 40 (SV40) T antigen construct to resolve these problems[6]. This model, the transgenic rat for adenocarcinoma of the prostate (TRAP), features development of high-grade prostatic intraepithelial neoplasia (HGPIN) from 4 weeks of age and androgen-dependent well-moderately differentiated adenocarcinomas with 100% incidences by the age of 15 weeks. These characteristics of the TRAP model have been shown to be

Received: 8 September 2013, Accepted: 28 October 2013
*Corresponding author: S Takahashi (e-mail: sattak@med.nagoya-cu.ac.jp)
Present: # Division of Cancer Prevention Research, National Cancer Center Research Institute, ****complete address****, Tokyo, Japan
Present: ## National Center for Geriatrics and Gerontology, ****complete address****, Obu, Japan
Present: ### Nagoya City Rehabilitation Center, ****complete address****, Nagoya, Japan
©2014 The Japanese Society of Toxicologic Pathology
This is an open-access article distributed under the terms of the Creative Commons Attribution Non-Commercial No Derivatives (by-nc-nd) License <http://creativecommons.org/licenses/by-nc-nd/3.0/>.

complete address
が必要ですのでお
知らせください。

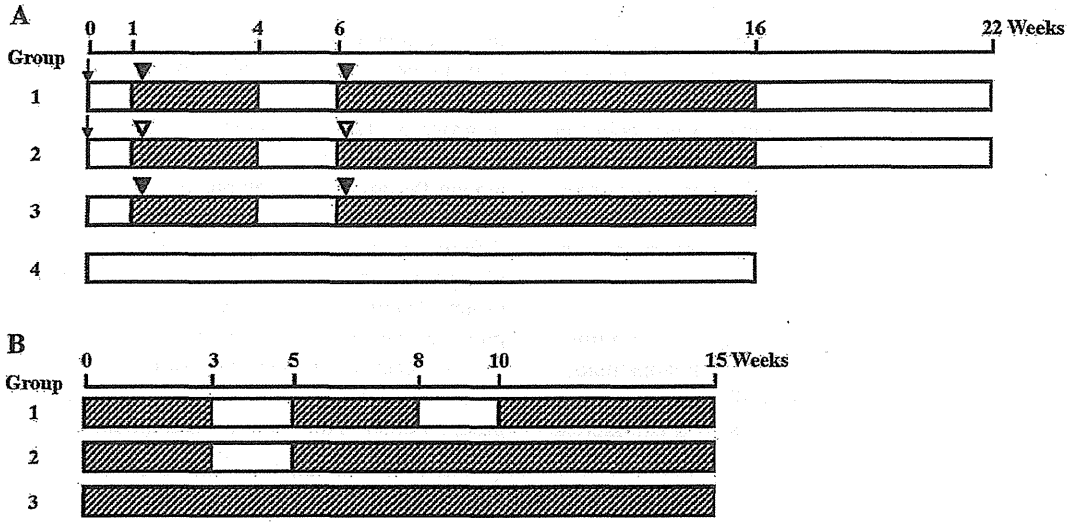

Fig. 1. Experimental design for experiments 1 (A) and 2 (B) for induction of invasive prostate adenocarcinomas in TRAP rats. The animals used were male TRAP rats that were 6 weeks of age at commencement of the study. Shaded, testosterone propionate, silicone rubber tube (40 mg); arrow, bilateral orchiectomy; filled arrowhead, DMAB 50 mg/kg b.w.; open arrowhead, vehicle (corn oil).

very suitable for evaluation of strategies for chemoprevention and treatment[7–10]. Microinvasive carcinomas characterized by a budding morphology from acini are observed in an age-dependent manner in TRAP rats, but these lesions are generally only 0.2–0.3 mm diameter in size and take over 35 weeks to develop[11]. We speculated that testosterone administration might be of paramount importance in the induction of invasive carcinoma in our transgenic rats based on our experience with the DMAB combined with TP-induced prostate carcinogenesis model. In the present study, we therefore assessed whether testosterone exposure might result in a high-grade invasive phenotype or metastatic lesions in TRAP rats.

Materials and Methods

Chemicals

TP was purchased from Sigma-Aldrich (St. Louis, MO, USA) and DMAB was obtained from Matsugaki Pharmaceutical Co. (Osaka, Japan). The purity of DMAB was >98%. Antibody for androgen receptor (AR) was obtained from Santa Cruz Biotechnology Inc (N-20, Santa Cruz, CA, USA). The antibody for Ki-67 was from Acris Antibodies GmbH (SP-6, Hiddenhausen, Germany).

Animals

Male heterozygous TRAP rats with a Sprague–Dawley genetic background were obtained from Oriental BioService Inc. (Minamiyamashiro, Kyoto, Japan) and were housed in plastic cages with hardwood chips in an air-conditioned room with a 12 h light/dark cycle at 23 ± 2°C and 50 ± 10% humidity. Food (Oriental MF; Oriental Yeast Co., Ltd., Tokyo, Japan) and tap water were available *ad libitum*. They were acclimatized for 1 week before use. Surgical treatments, such as orchiectomy and tube implantation, were carried out under deep isoflurane anesthesia. All animal experiments were performed under protocols approved by the Institutional Animal Care and Use Committee of the Nagoya City University Graduate School of Medical Sciences.

Experimental protocols

Experiment 1: A total of 24 male TRAP rats aged 6 weeks were randomly divided into four groups. Rats in groups 1 and 2 were treated with bilateral orchiectomy at day 0 of the experiment. Those in groups 1–3 underwent subcutaneous implantation of 2-cm-long silicone rubber tubes (Silascon®, inner diameter, 0.2 cm; outer diameter, 0.3 cm, Kaneka Medix Corporation, Osaka, Japan) containing 40 mg TP sealed at both ends with silicone rubber sealing compound (KE-42, Shin-Etsu Chemical Co., Ltd., Tokyo, Japan) into the interscapular region from weeks 1 to 4 and from weeks 6 to 16. The TP implants were replaced at 6-week intervals. Rats in groups 1 and 3 were subcutaneously given DMAB at a dose of 50 mg/kg body weight on the second day after TP tube implantation. No treatment was performed in rats of group 4, which served as controls. Animals were euthanized at weeks 16 and 22 after the beginning of the experiment (Fig.1A).

Experiment 2: A total of 24 heterozygous male TRAP rats aged 6 weeks were randomly divided into three groups. All were given TP implants in the same manner as in experiment 1 at day 0. The duration of TP administration was different among the groups; that is, TP was administered in experimental weeks 0–3, 5–8 and 10–15 in group 1 and

in experimental weeks 0–3 and 5–15 in group 2. Group 3 was continuously administered TP by implants throughout the experiment. The experiment was terminated at week 15 (Fig. 1B).

In both experiments, blood samples were collected from the abdominal aorta under deep anesthesia, and prostates were removed and fixed in formalin. For tissue preparation of prostate glands, four sagittal slices of the ventral prostate, two sagittal samples of the dorsolateral prostate including the urethra, and two transverse slices from each side of the anterior prostate including seminal vesicles were embedded in paraffin. Tissues were processed routinely and stained with hematoxylin and eosin for histopathological examination. Testosterone and estradiol levels in serum were analyzed using radioimmunoassays by a commercial laboratory (SRL, Inc., Tokyo, Japan).

Immunohistochemistry

Deparaffinized sections were incubated with diluted antibodies for AR and Ki-67. The immunohistochemical analysis was performed with a Discovery XT System (Ventana Medical Systems, Tucson, AZ, USA). Incubation with primary antibodies was carried out for 3 hours followed by a one hour incubation with biotinylated anti-rabbit secondary antibody (Vectastain ABC Kit Rabbit IgG, Vector Laboratories, Burlingame, CA, USA) and a DAB detection kit (Ventana Medical Systems) according to the manufacturer's instructions. Sections were counterstained with hematoxylin to facilitate orientation.

Immunofluorescence

Deparaffinized sections were autoclaved at 120°C for 20 min in antigen retrieval solution (Nichirei Biosciences Inc.) and then allowed to cool. Sections were incubated with 1% skim milk for 1 hour at room temperature. For double staining, anti-smooth muscle actin antibodies (1A4, dilution 1:1,000, mouse monoclonal, Dako) and anti-vimentin antibodies (EPR3776, dilution 1:400, rabbit monoclonal, Abcam) were simultaneously added to the slides and incubated for 1 hour at room temperature. After washing the slides with PBS, fluorescein-labeled goat anti mouse IgG (Life Technologies Corporation.) and tetramethylrhodamine-labeled goat anti-rabbit IgG (Life Technologies Corporation.) were added followed by incubation at room temperature for 1 hour. After washing the slides with PBS, the sections were mounted with Vectashield containing DAPI (Vector Laboratories) and subjected to fluorescence microscopy.

Results

Experiment 1

At week 16, foci of invasive adenocarcinoma with abundant collagenous stroma were found in lateral, dorsal and anterior prostates of groups 1–3 (Fig. 2A, B, D, E), along with minute ventral invasive carcinomas with minimal fibrous stroma. Cancer invasion into perineural spaces was also observed (Fig. 2E). Almost all of infiltrating carcinoma cells expressed AR (Fig. 2C, F). The incidences of invasive adenocarcinoma varied among the groups, tending to be higher in group 3 in all prostatic lobes (Table 1). Similarly, the number of invasive carcinoma foci was highest in group 3 (Table 1). There were no differences in histopathological characteristics of invasive adenocarcinomas among the groups. Development of small cell carcinomas of the prostate was sporadically noted, but there were no differences in incidence among the groups. No metastasis of cancer lesions to distant organs was found in any of the groups. Noninvasive adenocarcinomas in the ventral, lateral prostates were observed in all rats of groups 1–4.

At week 22, neoplastic lesions of the prostates were completely resolved with massive involution in all rats of groups 1 and 2. This indicated that all of the invasive adenocarcinomas developed in prostate glands were androgen-dependent (data not shown).

Experiment 2

The results of experiment 1 indicated that bilateral orchiectomy or DMAB administration did not deeply contribute to efficient induction of invasive adenocarcinomas. Thus, we focused on whether TP administration/withdrawal was important.

A significant increase of invasive adenocarcinoma development was observed in group 1, and this correlated well with the number of TP administration/withdrawal cycles in the lateral prostates (Table 2). Multicentric development of invasive adenocarcinoma foci with abundant collagenous stroma was found (Fig. 3A–D), and invasive cancer cells were observed in the stroma (Fig. 3E) and were positive for AR protein (Fig. 3F). Some invasive lesions consisted of cells with atrophic features, but more than 50% of these cells were labeled for Ki-67, suggesting that they were high-grade adenocarcinomas (Fig. 3G). Reactive stromal cells surrounding invasive cancers expressed both smooth muscle actin and vimentin and were therefore revealed to be cancer-associated myofibroblasts (Fig. 4). Noninvasive adenocarcinomas in the ventral and lateral prostates were found in all rats of groups 1–3.

Discussion

The TRAP rat features sequential progression from prostatic intraepithelial neoplasias (PINs) to noninvasive adenocarcinomas through prostate epithelial cell-specific expression of the SV40 T antigen regulated by the androgen-dependent probasin promoter. We have applied the TRAP rat model to validate the chemopreventive effects of a variety of chemicals, and cancer development in TRAP rats is very sensitive to chemicals that modulate the AR axis, such as flutamide, finasteride, resveratrol or angiotensin II receptor blockers [7, 9, 12]. These characteristics underly its acceptability to mimic early-stage hormone naïve human prostate cancer without an invasive phenotype.

In the present study, we established a novel rat model for invasive adenocarcinoma of the prostate in TRAP rats

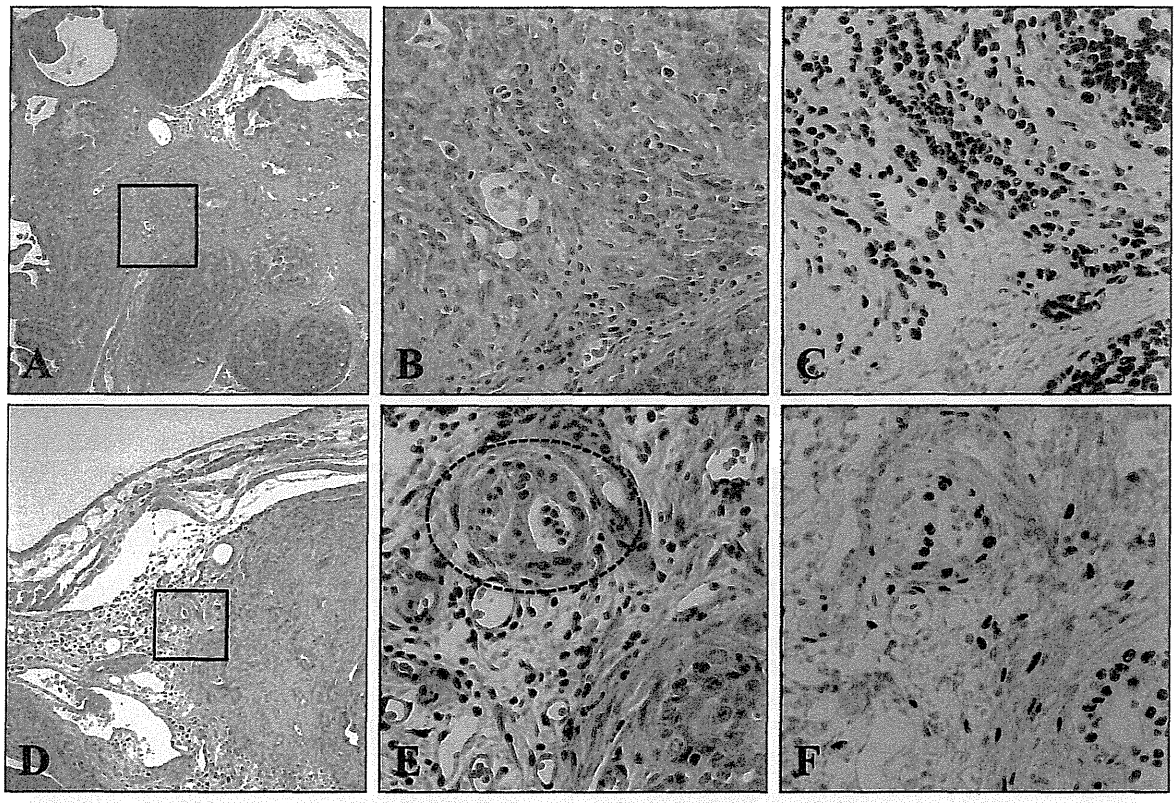

Fig. 2. Representative histopathological findings of invasive adenocarcinomas of the lateral prostate in group 3 (A–C) and anterior prostate in group 2 (D–F). Low (A, D) and high (B, E) magnifications of lateral and anterior prostates at week 16 after after the beginning of experiment 1. The rectangles in (A) and (D) represent the areas from (B) and (E), respectively. The dotted circle in (E) indicates perineural cancer invasion. (C, F) AR immunohistochemistry.

Table 1. Incidence and Multiplicity of Invasive Adenocarcinoma (at Week 16, Experiment 1)

Group	No. of rats	Lateral		Ventral		Dorsal		Anterior	
		Incidence (%)	No. of foci	Incidence (%)	No. of foci	Incidence (%)	No. of foci	Incidence (%)	No. of foci
1	5	1 (20)	0.20 ± 0.45	4 (80)	1.80 ± 1.64	1 (20)	0.20 ± 0.45	3 (60)	0.80 ± 0.84
2	4	2 (50)	1.00 ± 1.15	3 (75)	3.75 ± 3.78	1 (25)	0.25 ± 0.50	3 (75)	2.75 ± 3.10
3	4	4 (100)	4.00 ± 1.41[a,b]	4 (100)	6.00 ± 2.45[c]	3 (75)	1.00 ± 0.82	4 (100)	2.00 ± 0.82
4	5	2 (40)	0.40 ± 0.55	1 (20)	0.20 ± 0.45	0	-	2 (40)	0.40 ± 0.55

[a] P<0.001 vs groups 1 and 4; [b] P<0.01 vs group 2; [c] P<0.05 vs group.

Table 2. Incidence and Multiplicity of Invasive Adenocarcinoma (Experiment 2)

Group	No. of rats	Lateral		Ventral		Dorsal		Anterior	
		Incidence (%)	No. of foci	Incidence (%)	No. of foci	Incidence (%)	No. of foci	Incidence (%)	No. of foci
1	9	8 (89)	1.78 ± 1.10	8 (89)	4.22 ± 2.59**	2 (22)	0.44 ± 1.01	6 (67)	1.11 ± 1.05
2	9	7 (78)	1.67 ± 1.41	5 (56)	0.89 ± 0.93	0	-	7 (78)	0.78 ± 0.44
3	6	5 (83)	3.17 ± 1.72	2 (33)	0.33 ± 0.52	0	-	1 (17)	0.17 ± 0.41

** P<0.01 vs groups 2 and 3.

by intermittent TP administration (group 1 in experiment 2, shown in Fig. 1). The invasive carcinomas induced simulate human prostate cancer in several respects, such as perineural invasion and multicentric lesion development. To investigate mechanisms of prostate cancer progression, we previously combined administration of both DMAB and TP[5]. While several experiments were conducted with the aim of increasing the incidence of invasive cancer and shortening

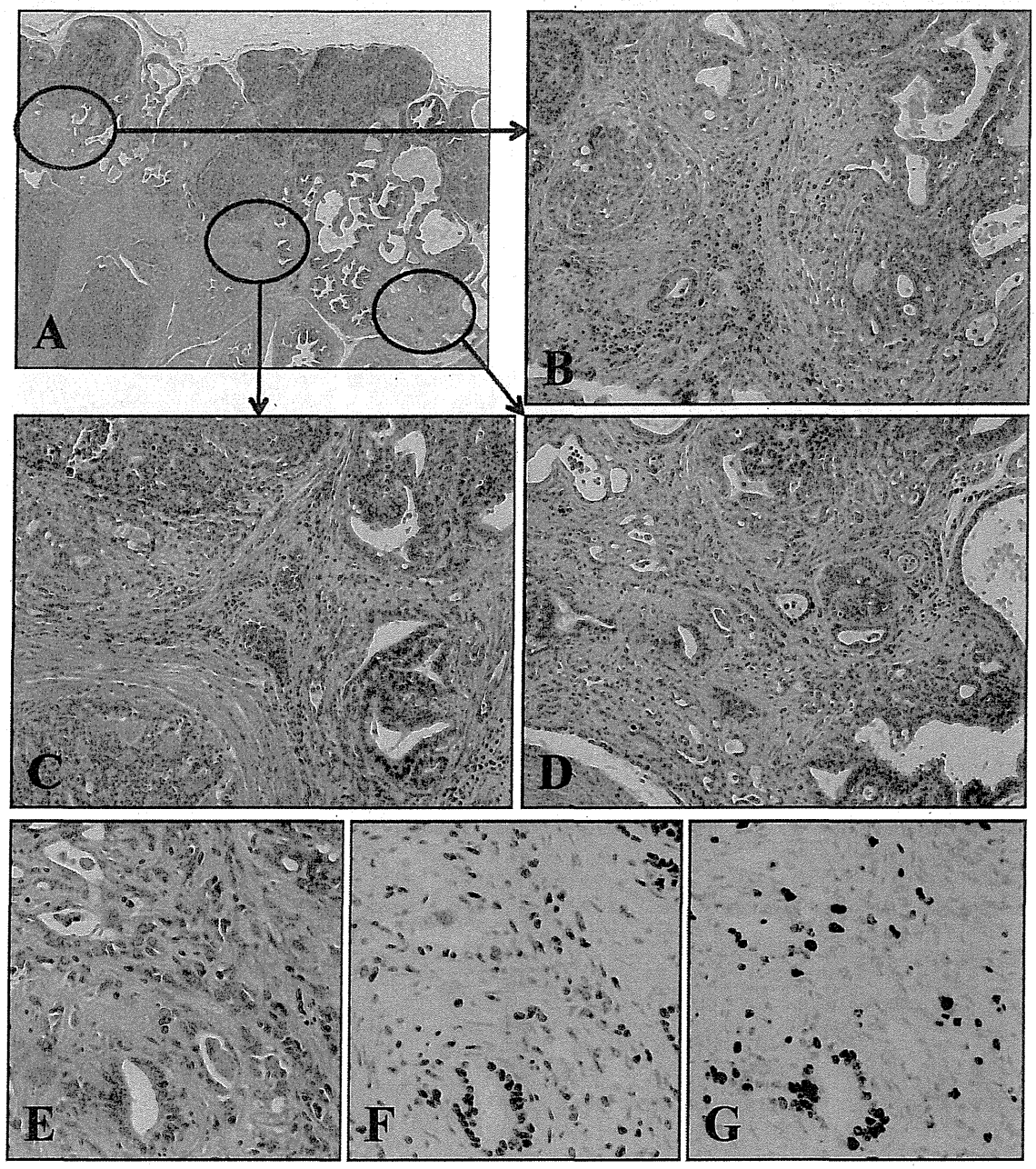

Fig. 3. Multicentric development of invasive adenocarcinomas in the lateral prostate in group 1 at week 15 after the beginning of experiment 2 (A–D). High magnifications of invasive adenocarcinoma with H&E (E), AR (F) and Ki-67 (G) staining.

the experimental period, none exceeded the DMAB + TP model in terms of the cancer incidence[13–16]. The new prostate carcinogenesis model documented here is characterized by invasive adenocarcinoma development at a high incidence in a short period without carcinogen administration. This rat model should enable us to investigate candidate chemopreventive agents for therapeutic effects as well as chemopreventive properties against prostate cancer.

We found that invasive adenocarcinoma incidences became greater as we increased the TP administration/withdrawal cycles for the TRAP rats. In our previous studies, testosterone induced invasive prostate adenocarcinomas in a dose- or duration-dependent manner after prostatic carcinogen treatment[14, 15]. However, continuous administration of testosterone alone earlier proved unable to cause development of invasive cancer with abundant reactive stromal tissue in the TRAP model[6,11]. The present results thus lead us to speculate that physiological destruction of the normal

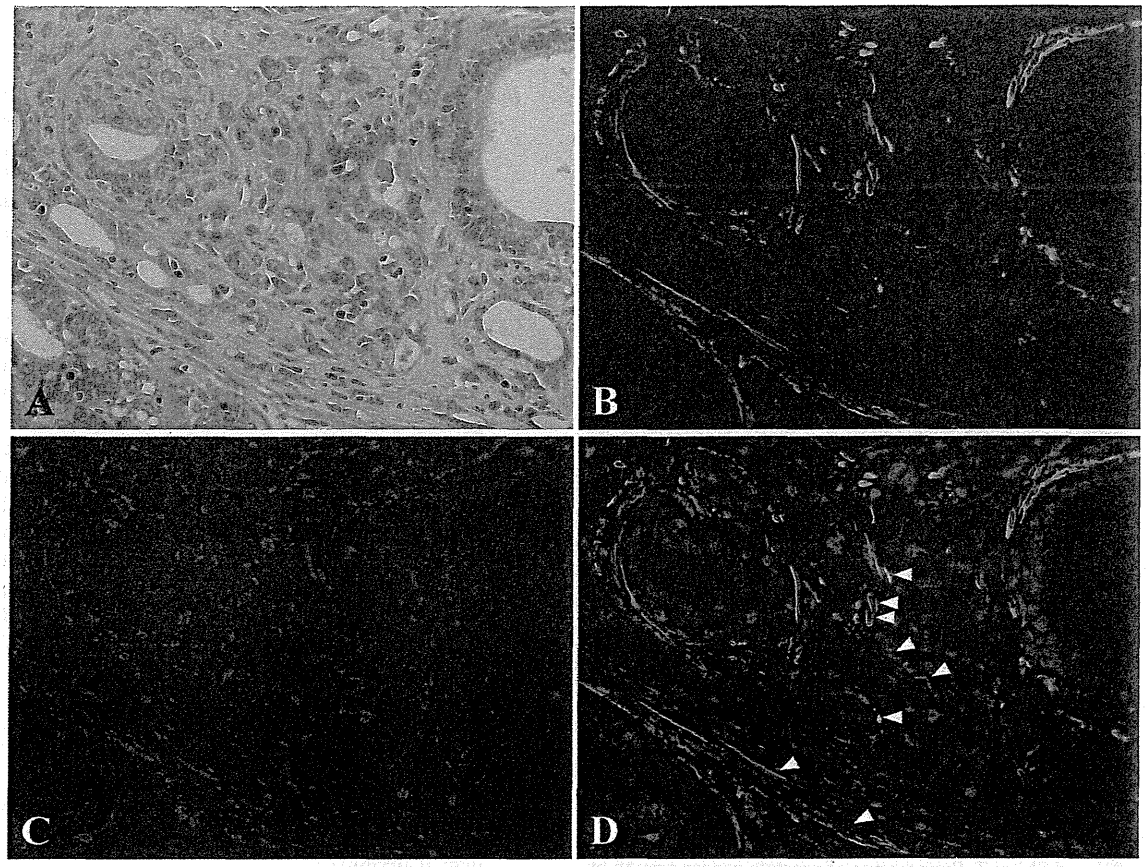

Fig. 4. Immunofluorescence analysis of an invasive adenocarcinoma in a lateral prostate. H&E (A). Immunofluorescence for smooth muscle actin (green, B) and vimentin (red, C), and a merged image (D). Blue, DAPI. Myofibroblasts coexpressing smooth muscle actin and vimentin are indicated by the arrowhead in (D).

acinar structure with stromal cell proliferation by androgen depletion plays an important role in the induction of invasive adenocarcinomas.

The process of primary cancer invasion, which initiates metastasis, is multifactorial and multistep and requires alteration of cell adherence, proteolytic degradation of extracellular matrix elements and tumor cell migration through tissue. Accumulating evidence has shown that stromal-epithelial interactions play critical roles in cancer progression[17–19]. The reactive tumor stroma mainly composed of cancer-associated fibroblasts (CAFs) including myofibroblasts, which are the predominant subpopulation of CAFs, is known to contribute to cancer development and progression[18–20]. Growth of myofibroblasts is reported to be stimulated by androgen[21]. TGFβ is one of the growth factors overexpressed in the prostate of rats after androgen ablation by orchiectomy[22]. TGFβ1 induces reactive oxygen species production via enhancement of NOX4 expression and may underly fibroblast-to-myofibroblast differentiation in the prostatic stroma[23], while myofibroblasts per se contribute to the production and activation of TGFβ1 and stromal cell-derived factor-1 (SDF-1)/CXCL12 by autocrine signaling loops[24]. Phosphoglycerate kinase-1 (PGK1), a downstream molecule of CXCL12-CXCR4 signaling, is upregulated in myofibroblasts, and this is involved in the enhanced proliferation and invasion of prostate cancer cells through activation of MMP, AKT and ERK pathways[25].

In conclusion, TP administration/withdrawal cycles appear to be of paramount importance to induction of invasive adenocarcinomas in the TRAP rat prostate. Our new rat prostate carcinogenesis model for invasive adenocarcinoma should provide opportunities to investigate molecular mechanisms of prostate cancer progression and may serve as a useful preclinical model for evaluating *in vivo* efficacy of preventive and therapeutic agents in terms of the tumor microenvironment.

Disclosure statement: The authors have no conflicts of interest.

Acknowledgments: This work was supported by a Grant-in-Aid for Cancer Research from the Ministry of Health, Labour and Welfare of Japan and a grant from the Society for Promotion of Pathology of Nagoya, Japan. The authors have no conflicts of interest regarding this research.

References

1. Siegel R, Naishadham D, and Jemal A. Cancer statistics, 2013. CA Cancer J Clin. **63**: 11–30. 2013. [Medline] [CrossRef]
2. Matsuda T, Marugame T, Kamo K, Katanoda K, Ajiki W, and Sobue T. Cancer incidence and incidence rates in Japan in 2006: Based on data from 15 population-based cancer registries in the monitoring of cancer incidence in Japan (MCIJ) project. Jpn J Clin Oncol. **42**: 139–147. 2012. [Medline] [CrossRef]
3. Zhang J, Dhakal IB, Zhao Z, and Li L. Trends in mortality from cancers of the breast, colon, prostate, esophagus, and stomach in East Asia: role of nutrition transition. Eur J Cancer Prev. **21**: 480–489. 2012. [Medline] [CrossRef]
4. Shirai T, Fukushima S, Ikawa E, Tagawa Y, and Ito N. Induction of prostate carcinoma in situ at high incidence in F344 rats by a combination of 3,2'-dimethyl-4-aminobiphenyl and ethinyl estradiol. Cancer Res. **46**: 6423–6426. 1986. [Medline]
5. Shirai T, Tamano S, Kato T, Iwasaki S, Takahashi S, and Ito N. Induction of invasive carcinomas in the accessory sex organs other than the ventral prostate of rats given 3,2'-dimethyl-4-aminobiphenyl and testosterone propionate. Cancer Res. **51**: 1264–1269. 1991. [Medline]
6. Asamoto M, Hokaiwado N, Cho YM, Takahashi S, Ikeda Y, Imaida K, and Shirai T. Prostate carcinomas developing in transgenic rats with SV40 T antigen expression under probasin promoter control are strictly androgen dependent. Cancer Res. **61**: 4693–4700. 2001. [Medline]
7. Seeni A, Takahashi S, Takeshita K, Tang M, Sugiura S, Sato SY, and Shirai T. Suppression of prostate cancer growth by resveratrol in the transgenic rat for adenocarcinoma of prostate (TRAP) model. Asian Pac J Cancer Prev. **9**: 7–14. 2008. [Medline]
8. Takahashi S, Takeshita K, Seeni A, Sugiura S, Tang M, Sato SY, Kuriyama H, Nakadate M, Abe K, Maeno Y, Nagao M, and Shirai T. Suppression of prostate cancer in a transgenic rat model via gamma-tocopherol activation of caspase signaling. Prostate. **69**: 644–651. 2009. [Medline] [CrossRef]
9. Takahashi S, Uemura H, Seeni A, Tang M, Komiya M, Long N, Ishiguro H, Kubota Y, and Shirai T. Therapeutic targeting of angiotensin II receptor type 1 to regulate androgen receptor in prostate cancer. Prostate. **72**: 1559–1572. 2012. [Medline] [CrossRef]
10. Long N, Suzuki S, Sato S, Naiki-Ito A, Sakatani K, Shirai T, and Takahashi S. Purple corn color inhibition of prostate carcinogenesis by targeting cell growth pathways. Cancer Sci. **104**: 298–303. 2013. [Medline] [CrossRef]
11. Cho YM, Takahashi S, Asamoto M, Suzuki S, Inaguma S, Hokaiwado N, and Shirai T. Age-dependent histopathological findings in the prostate of probasin/SV40 T antigen transgenic rats: lack of influence of carcinogen or testosterone treatment. Cancer Sci. **94**: 153–157. 2003. [Medline] [CrossRef]
12. Cho YM, Takahashi S, Asamoto M, Suzuki S, Tang M, and Shirai T. Suppressive effects of antiandrogens, finasteride and flutamide on development of prostatic lesions in a transgenic rat model. Prostate Cancer Prostatic Dis. **10**: 378–383. 2007. [Medline] [CrossRef]
13. Shirai T, Imaida K, Masui T, Iwasaki S, Mori T, Kato T, and Ito N. Effects of testosterone, dihydrotestosterone and estrogen on 3,2'-dimethyl-4-aminobiphenyl-induced rat prostate carcinogenesis. Int J Cancer. **57**: 224–228. 1994. [Medline] [CrossRef]
14. Shirai T, Sano M, Imaida K, Takahashi S, Mori T, and Ito N. Duration dependent induction of invasive prostatic carcinomas with pharmacological dose of testosterone propionate in rats pretreated with 3,2'-dimethyl-4-aminobiphenyl and development of androgen-independent carcinomas after castration. Cancer Lett. **83**: 111–116. 1994. [Medline] [CrossRef]
15. Shirai T, Tamano S, Sano M, Imaida K, Hagiwara A, Futakuchi M, Takahashi S, and Hirose M. Site-specific effects of testosterone propionate on the prostate of rat pretreated with 3,2'-dimethyl-4-aminobiphenyl: dose-dependent induction of invasive carcinomas. Jpn J Cancer Res. **86**: 645–648. 1995. [Medline] [CrossRef]
16. Cui L, Mori T, Takahashi S, Imaida K, Akagi K, Yada H, Yaono M, and Shirai T. Slight promotion effects of intermittent administration of testosterone propionate and/or diethylstilbestrol on 3,2'-dimethyl-4-aminobiphenyl-initiated rat prostate carcinogenesis. Cancer Lett. **122**: 195–199. 1998. [Medline] [CrossRef]
17. Valastyan S, and Weinberg RA. Tumor metastasis: molecular insights and evolving paradigms. Cell. **147**: 275–292. 2011. [Medline] [CrossRef]
18. Barron DA, and Rowley DR. The reactive stroma microenvironment and prostate cancer progression. Endocr Relat Cancer. **19**: R187–R204. 2012. [Medline] [CrossRef]
19. Otranto M, Sarrazy V, Bonte F, Hinz B, Gabbiani G, and Desmouliere A. The role of the myofibroblast in tumor stroma remodeling. Cell Adh Migr. **6**: 203–219. 2012. [Medline] [CrossRef]
20. Orimo A, and Weinberg RA. Heterogeneity of stromal fibroblasts in tumors. Cancer Biol Ther. **6**: 618–619. 2007. [Medline] [CrossRef]
21. Webber MM, Trakul N, Thraves PS, Bello-DeOcampo D, Chu WW, Storto PD, Huard TK, Rhim JS, and Williams DE. A human prostatic stromal myofibroblast cell line WPMY-1: a model for stromal-epithelial interactions in prostatic neoplasia. Carcinogenesis. **20**: 1185–1192. 1999. [Medline] [CrossRef]
22. Desai KV, and Kondaiah P. Androgen ablation results in differential regulation of transforming growth factor-β isoforms in rat male accessory sex organs and epididymis. J Mol Endocrinol. **24**: 253–260. 2000. [Medline] [CrossRef]
23. Sampson N, Koziel R, Zenzmaier C, Bubendorf L, Plas E, Jansen-Durr P, and Berger P. ROS signaling by NOX4 drives fibroblast-to-myofibroblast differentiation in the diseased prostatic stroma. Mol Endocrinol. **25**: 503–515. 2011. [Medline] [CrossRef]
24. Kojima Y, Acar A, Eaton EN, Mellody KT, Scheel C, Ben-Porath I, Onder TT, Wang ZC, Richardson AL, Weinberg RA, and Orimo A. Autocrine TGF-β and stromal cell-derived factor-1 (SDF-10 signaling drives the evolution of tumor-promoting mammary stromal myofibroblasts. Proc Natl Acad Sci USA. **107**: 20009–20014. 2010. [Medline] [CrossRef]
25. Wang J, Ying G, Wang J, Jung Y, Lu J, Zhu J, Pienta KJ, and Taichman RS. Characterization of phosphoglycerate kinase-1 expression of stromal cells derived from tumor microenvironment in prostate cancer progression. Cancer Res. **70**: 471–480. 2010. [Medline] [CrossRef]

ARTICLES

Adiponectin and AdipoR1 regulate PGC-1α and mitochondria by Ca^{2+} and AMPK/SIRT1

Masato Iwabu[1,2*], Toshimasa Yamauchi[1,2*], Miki Okada-Iwabu[1,2*], Koji Sato[6], Tatsuro Nakagawa[7], Masaaki Funata[1], Mamiko Yamaguchi[1], Shigeyuki Namiki[3], Ryo Nakayama[1], Mitsuhisa Tabata[8], Hitomi Ogata[9], Naoto Kubota[1], Iseki Takamoto[1], Yukiko K. Hayashi[10], Naoko Yamauchi[4], Hironori Waki[1], Masashi Fukayama[4], Ichizo Nishino[10], Kumpei Tokuyama[9], Kohjiro Ueki[1], Yuichi Oike[8], Satoshi Ishii[5], Kenzo Hirose[3], Takao Shimizu[5], Kazushige Touhara[6,7] & Takashi Kadowaki[1]

Adiponectin is an anti-diabetic adipokine. Its receptors possess a seven-transmembrane topology with the amino terminus located intracellularly, which is the opposite of G-protein-coupled receptors. Here we provide evidence that adiponectin induces extracellular Ca^{2+} influx by adiponectin receptor 1 (AdipoR1), which was necessary for subsequent activation of Ca^{2+}/calmodulin-dependent protein kinase kinase β (CaMKKβ), AMPK and SIRT1, increased expression and decreased acetylation of peroxisome proliferator-activated receptor γ coactivator-1α (PGC-1α), and increased mitochondria in myocytes. Moreover, muscle-specific disruption of AdipoR1 suppressed the adiponectin-mediated increase in intracellular Ca^{2+} concentration, and decreased the activation of CaMKK, AMPK and SIRT1 by adiponectin. Suppression of AdipoR1 also resulted in decreased PGC-1α expression and deacetylation, decreased mitochondrial content and enzymes, decreased oxidative type I myofibres, and decreased oxidative stress-detoxifying enzymes in skeletal muscle, which were associated with insulin resistance and decreased exercise endurance. Decreased levels of adiponectin and AdipoR1 in obesity may have causal roles in mitochondrial dysfunction and insulin resistance seen in diabetes.

Adiponectin (encoded by *Adipoq*)[1–4] is an anti-diabetic and anti-atherogenic adipokine. Plasma adiponectin levels are decreased in obesity, insulin resistance, and type 2 diabetes[5]. Administration of adiponectin has been shown to cause glucose-lowering effects and ameliorate insulin resistance in mice[6–8]. Conversely, adiponectin-deficient mice exhibit insulin resistance and diabetes[9,10]. This insulin-sensitizing effect of adiponectin seems to be mediated by an increase in fatty acid oxidation by activation of AMP-activated protein kinase (AMPK)[11–13] and also by peroxisome proliferator-activated receptor α (PPARα)[14,15].

We previously reported the cloning of complementary DNAs encoding adiponectin receptors 1 and 2 (*Adipor1* and *Adipor2*) by expression cloning[16]. AdipoR1 is abundantly expressed in skeletal muscle and liver, whereas AdipoR2 is predominantly expressed in the liver. Both receptors are predicted to contain seven-transmembrane domains[16], but to be structurally and functionally distinct from G-protein-coupled receptors[17–19]. Adiponectin receptors may thus be thought to comprise a new receptor family.

We previously showed using *Adipor1* and/or *Adipor2* knockout mice that AdipoR1 and AdipoR2 act as the major receptors for adiponectin *in vivo*, and have important roles in the regulation of glucose and lipid metabolism, inflammation and oxidative stress *in vivo*[20]. Moreover, in the liver, AdipoR1 activated AMPK pathways and AdipoR2 activated PPARα pathways[20]. Therefore, identification of the 'missing link' between adiponectin receptors and adiponectin-activated key molecules is an important next step towards our understanding of the actions of adiponectin.

Insulin resistance has been reported to be associated with mitochondrial dysfunction[21]. However, the exact cause of mitochondrial dysfunction has yet to be ascertained. To clarify whether decreased adiponectin/AdipoR1 signalling could be associated with mitochondrial dysfunction, we analysed muscle-specific *Adipor1*-knockout (muscle-R1KO) mice, and attempted to determine the signalling mechanisms by which adiponectin/AdipoR1 would exert their biological effects.

Decreased PGC-1α and mitochondria in muscle-R1KO

Muscle-R1KO mice showed decreased phosphorylation of AMPK (Fig. 1a). Moreover, the administration of adiponectin increased the phosphorylation of AMPK in the muscle of control littermates but not in those of muscle-R1KO mice (Supplementary Fig. 1a), whereas adiponectin increased the phosphorylation of AMPK in the liver of both genotypes (Supplementary Fig. 1b). Muscle-R1KO mice also exhibited decreased molecules involved in mitochondrial biogenesis, such as PGC-1α[22], at both messenger RNA (*Ppargc1a*) (Fig. 1b) and protein levels (Fig. 1c). Adiponectin increased the expression levels of *Ppargc1a* in muscles of control littermates but not in those of muscle-R1KO mice (Supplementary Fig. 1c).

Muscle-R1KO mice showed decreases in molecules involved in mitochondrial biogenesis such as oestrogen-related receptor α (*Esrra*)[23], molecules involved in transcription such as nuclear respiratory factor 1 (*Nrf1*), and molecules involved in mitochondrial DNA replication/translation such as mitochondrial transcription factor A (*Tfam*)

[1]Department of Diabetes and Metabolic Diseases, Graduate School of Medicine, [2]Department of Integrated Molecular Science on Metabolic Diseases, 22nd Century Medical and Research Center, [3]Department of Neurobiology, Graduate School of Medicine, [4]Department of Pathology, Graduate School of Medicine, [5]Department of Biochemistry and Molecular Biology, Faculty of Medicine, The University of Tokyo, Tokyo 113-0033, Japan. [6]Department of Applied Biological Chemistry, Graduate School of Agricultural and Life Sciences, The University of Tokyo, Tokyo 113-8657, Japan. [7]Department of Integrated Biosciences, The University of Tokyo, Chiba 277-8562, Japan. [8]Department of Molecular Genetics, Graduate School of Medical Sciences, Kumamoto University, Kumamoto 860-0811, Japan. [9]Graduate School of Comprehensive Human Sciences, University of Tsukuba, Tsukuba 305-8577, Japan. [10]Department of Neuromuscular Research, National Institute of Neuroscience, National Center of Neurology and Psychiatry, Kodaira, Tokyo 187-8502, Japan.
*These authors contributed equally to this work.

©2010 Macmillan Publishers Limited. All rights reserved

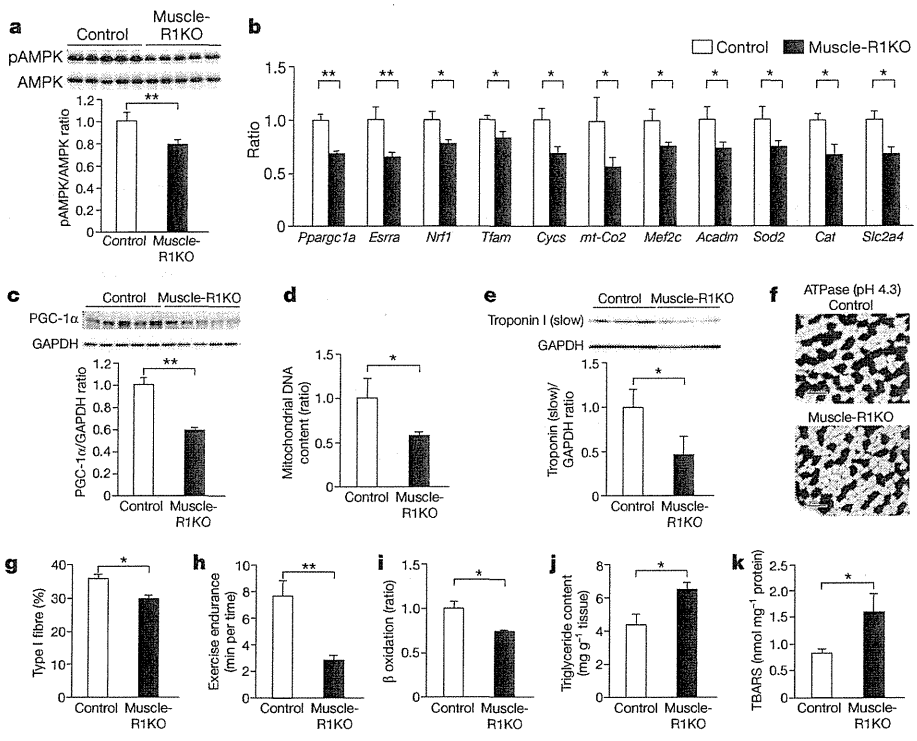

Figure 1 | Decreased mitochondria, oxidative type I myofibres and exercise capacity in skeletal muscle of muscle-R1KO mice. **a–k**, Phosphorylation and amount of AMPK (**a**), *Ppargc1a*, *Esrra*, *Nrf1*, *Tfam*, *Cycs*, *mt-Co2*, *Mef2c*, *Acadm*, *Sod2*, *Cat* and *Slc2a4* mRNA levels (**b**), PGC-1α protein levels (**c**), mitochondrial content as assessed by mitochondrial DNA copy number (**d**), amounts of troponin I (slow) protein (**e**), ATPase (pH 4.3 for type I fibres) staining of soleus muscles (scale bars, 100 μm) (**f**), quantification of type I fibres (**g**) based on fibre-type analyses (**f**), exercise endurance (**h**), β oxidation (**i**), triglyceride content (**j**), and TBARS (**k**) in skeletal muscle (**a–g**, **i–k**) obtained from control or muscle-R1KO after 5 h fasting. All values are presented as mean ± s.e.m. $n = 5–12$, $^{*}P < 0.05$ and $^{**}P < 0.01$ compared to control mice.

(Fig. 1b). Moreover, the expression levels of several oxidative phosphorylation and other mitochondrial genes were significantly reduced in muscle-R1KO mice, including cytochrome *c* (*Cycs*), and cytochrome *c* oxidase subunit II (*mt-Co2*) (Fig. 1b). Furthermore, muscle-R1KO mice had a decreased mitochondrial DNA content (Fig. 1d).

Mitochondrial function was assessed by measuring the enzymatic activities of Cox (Supplementary Fig. 2a) and succinate dehydrogenase (SDH) (Supplementary Fig. 2b). Staining of soleus muscle sections revealed a lower number of Cox- and SDH-positive muscle fibres and a decreased intensity of Cox and SDH staining in muscle-R1KO mice (Supplementary Fig. 2a, b).

Decreased type I fibres and exercise capacity in muscle-R1KO

Muscle-R1KO mice had decreased molecules involved in type I fibre[24] differentiation myocyte enhancer factor 2C (*Mef2c*)[25] (Fig. 1b) as well as the type I fibre marker troponin I (slow) (Fig. 1e). In contrast, muscle-R1KO mice had almost the same expression levels of MHCIIa, MHCIIx and MHCIIb as those seen in control mice (Supplementary Fig. 2c–e), indicating a reduction in oxidative, high endurance fibres in muscle-R1KO mice. These findings were consistent with the histological analysis performed (Fig. 1f, g). In soleus muscle of muscle-R1KO mice, type I fibres were reduced by 20% (Fig. 1g).

To study the effect of *Adipor1* ablation on skeletal muscle function in intact animals, we challenged control and muscle-R1KO mice with involuntary physical-exercise-assessed muscle endurance by treadmill running. Muscle endurance was significantly lower for muscle-R1KO mice than control mice (Fig. 1h).

We next examined the expression of metabolic genes and found that molecules involved in fatty-acid oxidation, such as medium-chain acyl-CoA dehydrogenase (*Acadm*), were significantly decreased in muscle-R1KO mice (Fig. 1b), which was associated with decreased β oxidation (Fig. 1i) and increased triglyceride content (Fig. 1j) in skeletal muscle.

Muscle-R1KO mice exhibited decreased expression levels of mitochondrial and cytoplasmic oxidative-stress-detoxifying genes such as manganese superoxide dismutase (*Sod2*) (Fig. 1b) and catalase (*Cat*) (Fig. 1b), respectively, and increased oxidative stress such as thiobarbituric acid reactive substance (TBARS) (Fig. 1k) in muscle. Expression of the insulin-sensitive glucose transporter 4 (*Slc2a4*) was reduced in muscle-R1KO mice (Fig. 1b).

Insulin resistance in muscle-R1KO mice

Plasma glucose and insulin levels after glucose administration were significantly higher in muscle-R1KO mice than in control mice (Fig. 2a, b). The capacities of muscle-R1KO mice to regulate plasma glucose levels after a bolus of insulin were significantly decreased as compared with control mice (Fig. 2c).

We performed a hyperinsulinaemic-euglycaemic clamp experiment. Disruption of *Adipor1* in muscle did not significantly alter endogenous glucose production, whereas it significantly decreased the glucose disposal rate and the glucose infusion rate, indicating decreased insulin sensitivity in muscle (Fig. 2d–f).

In agreement with the data obtained from the hyperinsulinaemic-euglycaemic clamps, decreased tyrosine phosphorylation of IRS-1 (Fig. 2g) and decreased phosphorylation of Ser 473 in Akt (Fig. 2h) stimulated with insulin in skeletal muscle of muscle-R1KO mice were found, which seemed to be associated with increased phosphorylation of S6K1 (Fig. 2i) and JNK (Fig. 2j). Ser 302 in mice IRS-1 has been reported to be phosphorylated by JNK[26], and the phosphorylation of Ser 636/639 has been reported to be mediated by mTOR and S6K1 pathways[27], both of which would result in inhibition of insulin signalling. The amounts of Ser 302 and Ser 636/639 phosphorylation in IRS-1 were increased in skeletal muscle of muscle-R1KO mice (Fig. 2k, l).

CaMKKβ is required for adiponectin/AdipoR1-induced PGC-1α

We next investigated the molecular mechanisms by which muscle-R1KO mice exhibited these phenotypes described earlier. Incubation of C2C12 myocytes with 30 μg ml^{-1} adiponectin increased mitochondrial DNA content (Fig. 3a). AMPK activity is dependent on the phosphorylation of AMPKα(Thr 172) in its activation loop by AMPK kinases (AMPKKs)[13,28]. LKB1 and CaMKKβ are known to be two major AMPKKs present in a variety of tissues and cells[13,29,30]. Suppression of AdipoR1 or CaMKKβ, or both AMPKα1 and AMPKα2 or PGC-1α expression by each specific short interfering RNA (siRNA) (Supplementary Fig. 3a–e) markedly reduced the increases in mitochondrial DNA content induced by adiponectin (Fig. 3a). In contrast, the suppression of AdipoR2 expression by

©2010 Macmillan Publishers Limited. All rights reserved

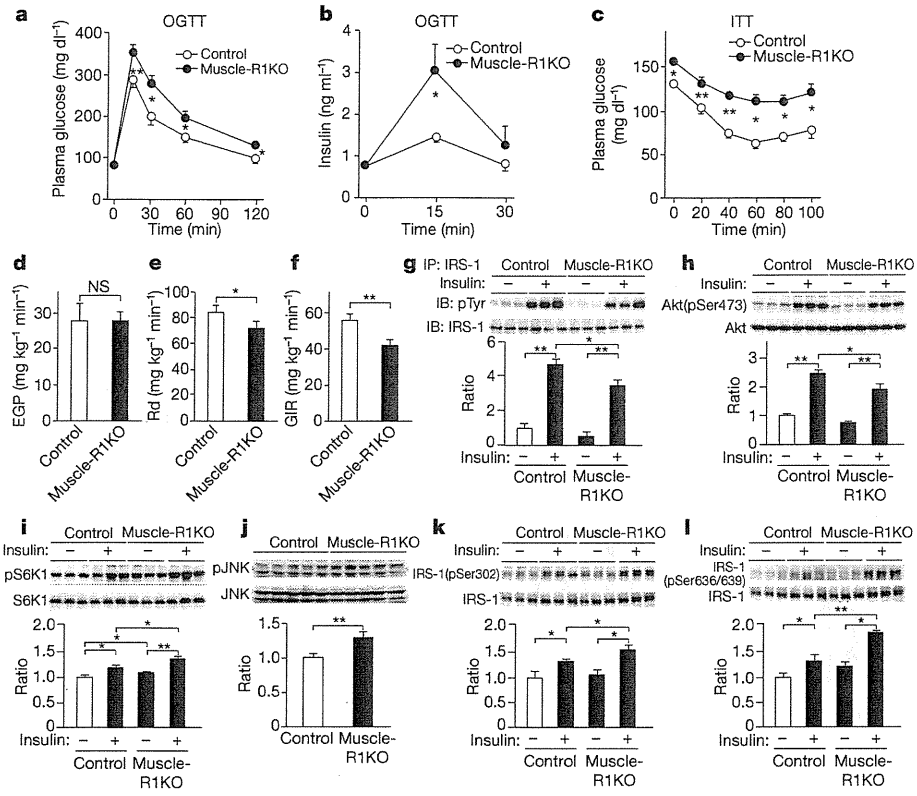

Figure 2 | Mechanisms of abnormal glucose and insulin homeostasis in muscle-R1KO mice. **a–f**, Plasma glucose (**a**, **c**) and plasma insulin (**b**) during an oral glucose tolerance test (OGTT) (1.5 g glucose per kg body weight) (**a**, **b**) or during an insulin tolerance test (ITT) (0.25 U insulin per kg body weight) (**c**), endogenous glucose production (EGP) (**d**), rates of glucose disposal (Rd) (**e**) and glucose infusion rate (GIR) (**f**) during a hyperinsulinaemic-euglycaemic clamp study in control and muscle-R1KO mice. **g–l**, Phosphorylation of tyrosine (pTyr) (**g**), Ser 302 (**k**) and Ser 636/639 (**l**) in IRS-1, phosphorylation and amount of Akt (**h**), S6K1 (**i**) and JNK (**j**) in skeletal muscle treated with or without insulin (0.3 U per kg body weight) for 7.5 min in control and muscle-R1KO mice after 5 h fasting. IB, immunoblot; IP, immunoprecipitate. All values are presented as mean ± s.e.m. $n = 6$–15 from 3–5 independent experiments, $^{*}P < 0.05$ and $^{**}P < 0.01$ compared to control or as indicated. NS, not significant.

specific siRNA (Supplementary Fig. 3f) failed to significantly reduce mitochondrial biogenesis induced by adiponectin (Fig. 3a).

Suppression of AdipoR1 or CaMKKβ expression by each specific siRNA (Supplementary Fig. 3a, b) greatly reduced the increase in PGC-1α expression induced by adiponectin (Fig. 3b). Interestingly, the suppression of AMPKα1 and AMPKα2 expression by each specific siRNA (Supplementary Fig. 3c, d) failed to significantly reduce PGC-1α expression induced by adiponectin (Fig. 3b), suggesting that PGC-1α expression was induced by adiponectin via an AdipoR1- and CaMKKβ-dependent yet AMPK-independent pathway.

PGC-1α has been reported to be activated by AMPK via phosphorylation[31] and by deacetylation through SIRT1 activation[32]. We next addressed the possibility that AMPK activated by adiponectin and AdipoR1 could regulate PGC-1α activities. Treatment of C2C12 myocytes with adiponectin decreased PGC-1α acetylation after 2 h of treatment (Fig. 3c). Suppression of AdipoR1 or both AMPKα1 and AMPKα2 or SIRT1 expression by each specific siRNA (Supplementary Fig. 3a, c, d, g) largely abrogated the decrease in PGC-1α acetylation induced by adiponectin (Fig. 3c). The PGC-1α-2A mutant lacking the two AMPK phosphorylation sites[31] showed markedly reduced PGC-1α deacetylation and mitochondrial biogenesis with adiponectin (Fig. 3d, e).

Adiponectin failed to induce mitochondrial biogenesis further in the C2C12 myocytes expressing PGC-1α-R13 in which 13 of the potential lysine acetylation sites were mutated into arginine[32] (Fig. 3f). Because the capacity for undergoing acetylation is impaired in the PGC-1α-R13 mutant, these data are consistent with the dependence of adiponectin on SIRT1-mediated deacetylation of PGC-1α in activating PGC-1α.

SIRT1 deacetylase activity has been reported to be driven by NAD^+ levels[32,33]. Adiponectin increased the NAD^+/NADH ratio in C2C12 myocytes (Fig. 3g). Muscle-R1KO mice also showed increased PGC-1α acetylation (Fig. 3h) and decreased the NAD^+/NADH ratio stimulated with adiponectin (Fig. 3i) *in vivo*. These data indicated that the total activity as assessed by multiplying expression and deacetylation of PGC-1α is markedly reduced in muscle-R1KO mice (Supplementary Fig. 4).

Adiponectin induces Ca^{2+} influx by AdipoR1

Interestingly, treatment of C2C12 myocytes with adiponectin resulted in an increase in the intracellular Ca^{2+} concentration measured by fura-2-based fluorescent imaging (Fig. 4a). C2C12 myocytes showed responses to adiponectin in a dose-dependent manner (data not shown). Removal of extracellular free Ca^{2+} by EGTA almost completely abolished the adiponectin-induced Ca^{2+} response (Fig. 4a), whereas EGTA had no effect on the ATP-induced intracellular Ca^{2+} release (data not shown). Suppression of AdipoR1 expression using a specific siRNA (Fig. 4b) largely reduced the calcium response of C2C12 myocytes to adiponectin (Fig. 4c, d). These results indicate that the influx of extracellular Ca^{2+} after adiponectin treatment of C2C12 myocytes is mediated by AdipoR1.

To study further the importance of AdipoR1 for adiponectin-induced Ca^{2+} response in the gain-of-function experiments, we expressed AdipoR1 in *Xenopus laevis* oocytes (Fig. 4e). The increase in intracellular calcium levels stimulated with adiponectin was detected by monitoring Ca^{2+}-activated Cl^- currents in AdipoR1 complementary-RNA-injected oocytes (Fig. 4f, g). The responses were not observed in control oocytes (Fig. 4g). We studied the effect of removal of extracellular free Ca^{2+} by EGTA on the Ca^{2+}-activated Cl^- current response to adiponectin of *Xenopus* oocytes expressing AdipoR1. We found that the removal of extracellular free Ca^{2+} by EGTA almost completely abolished the Ca^{2+}-activated Cl^- current response to adiponectin of *Xenopus* oocytes expressing AdipoR1 (Fig. 4g), indicating that these responses were dependent on extracellular Ca^{2+}.

Adiponectin-induced Ca^{2+} influx is important for its actions

Incubation of C2C12 myocytes with adiponectin increased the phosphorylation of the AMPK α-subunit at Thr 172, and EGTA partially suppressed adiponectin-induced increased AMPK phosphorylation (Fig. 5a). As expected, EGTA almost completely abolished ionomycin-dependent phosphorylation of AMPK, whereas EGTA had no effect on 5-aminoimidazole-4-carboxamide-1-β-D-riboside (AICAR)-induced phosphorylation of AMPK in C2C12 myocytes (Fig. 5a).

Suppression of CaMKKβ or LKB1 expression by each specific siRNA (Supplementary Fig. 3b, h) significantly reduced the increases in

©2010 Macmillan Publishers Limited. All rights reserved

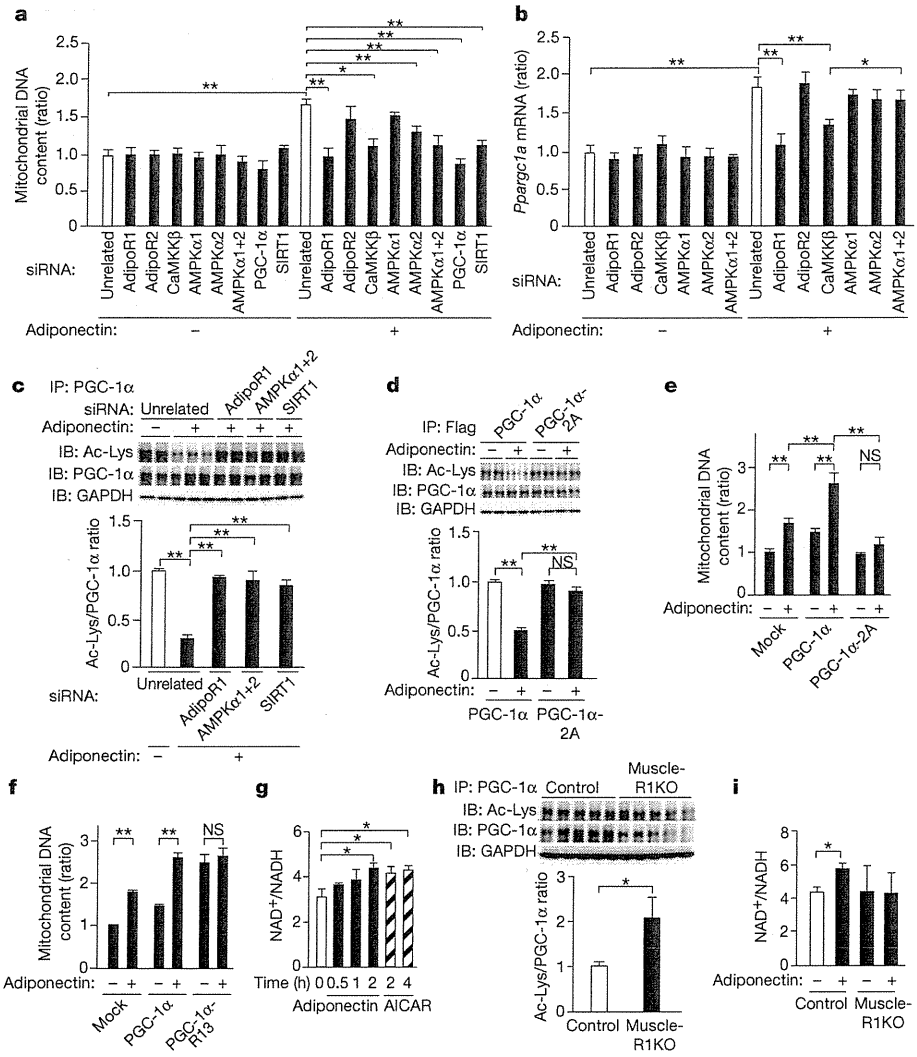

Figure 3 | Adiponectin/AdipoR1 increase PGC-1α expression and activity, and mitochondrial biogenesis in C2C12 myocytes. **a–i**, Mitochondrial content as assessed by mitochondrial DNA copy number (**a**, **e**, **f**), *Ppargc1a* mRNA levels (**b**), acetyl-lysine (Ac-Lys) levels checked on PGC-1α or Flag immunoprecipitates (**c**, **d**, **h**), NAD^+/NADH ratio (**g**, **i**) in C2C12 myocytes treated with adiponectin for the times indicated (**g**), in C2C12 myocytes transfected with the indicated siRNA duplex (**a–c**), in C2C12 myocytes transfected with the wild-type or the 2A mutant form of PGC-1α (**d**, **e**) or the R13 mutant form of PGC-1α (**f**) treated with 10 μg ml^{-1} adiponectin for 48 h (**a**, **e**, **f**) or for 1.5 h (**b**) or 2 h (**c**, **d**), or in skeletal muscle from control or muscle-R1KO mice treated with or without adiponectin (**h**, **i**). The supernatant was blotted against GAPDH as an input control (**c**, **d**, **h**). C2C12 myocytes were used after myogenic differentiation in all experiments. All values are presented as mean ± s.e.m. $n = 5–10$, $^*P < 0.05$ and $^{**}P < 0.01$ compared to control or unrelated siRNA or as indicated.

phosphorylation of AMPK induced by adiponectin (Fig. 5b). Although the AMPK inhibitor AraA only tended to reduce adiponectin-induced PGC-1α expression, Ca^{2+} removal by EGTA or inhibition of CaMKKβ with its selective inhibitor STO-609 (ref. 34) effectively and almost completely abolished increased PGC-1α expression stimulated with adiponectin in C2C12 myocytes (Fig. 5c), as removal of extracellular Ca^{2+} effectively abolishes the Ca^{2+} signal evoked by adiponectin (Fig. 4a).

Finally, we examined whether adiponectin-induced Ca^{2+} influxes into skeletal muscle might be impaired in muscle-R1KO mice through *in vivo* imaging[35,36]. We found that whereas treatment of soleus muscle with adiponectin resulted in an increase in the intracellular Ca^{2+} concentration as measured by fura-2-based fluorescent imaging in control mice, muscle-R1KO mice almost completely abrogated the calcium response of soleus muscle to adiponectin (Fig. 5d–f), consistent with the observation that adiponectin significantly increased the phosphorylation of CaMKI[37,38], an intracellular substrate of CaMKKβ, by AdipoR1 in skeletal muscle *in vivo* (Supplementary Fig. 5).

We also attempted to examine whether simultaneous activation of Ca^{2+} signalling and AMPK/SIRT1 pathways by exercise, independent of AdipoR1, could rescue phenotype in muscle-R1KO mice. Two weeks of exercise significantly ameliorated insulin resistance, and increased mitochondrial content and function such as citrate synthase activities in muscles of muscle-R1KO mice (Fig. 6a–d).

Discussion

Here we provide evidence that muscle-R1KO mice exhibit decreased mitochondrial content and enzymes. PGC-1α is a key regulator of mitochondrial content and function. Expression of PGC-1α has been reported to be modulated in several physiological contexts, for example, in skeletal muscle in response to exercise partly by increased Ca^{2+} signalling via molecules such as CaMK and CREB[39]. Activities of PGC-1α have also been reported to be modulated by several kinds of PGC-1α modifications, such as phosphorylation by AMPK[31] and deacetylation by AMPK and SIRT1[32]. AMPK and SIRT1 could also be activated by exercise. We have demonstrated that muscle-R1KO mice exhibit decreased PGC-1α expression as well as decreased deacetylation of PGC-1α. Consistent with this, adiponectin induced Ca^{2+} influx by AdipoR1, thereby activating CaMKKβ, which led to increased PGC-1α expression. Moreover, adiponectin/AdipoR1 activated AMPK and SIRT1, thereby inducing PGC-1α deacetylation. These data indicated that adiponectin and AdipoR1 stimulate increases in both the expression and activation of PGC-1α, in a similar fashion to exercise (Fig. 6e).

Although the degree of decreased PGC-1α expression was approximately 40% in muscle-R1KO mice, the extent of decreased mitochondrial biogenesis and decreased exercise endurance were comparable to those observed in muscle-specific PGC-1α-knockout mice[40], which may be explained by the finding that adiponectin and AdipoR1 increase not only PGC-1α expression but also PGC-1α activity (Fig. 6e).

Importantly, decreases in the expression of AdipoR1 and PGC-1α and mitochondrial DNA content were also observed in type 2 diabetic patients[41] and individuals at increased risk of developing diabetes owing to their family history[42], as well as in obese diabetic *db/db* mice (Supplementary Fig. 6a–c). These data indicate that decreased

©2010 Macmillan Publishers Limited. All rights reserved

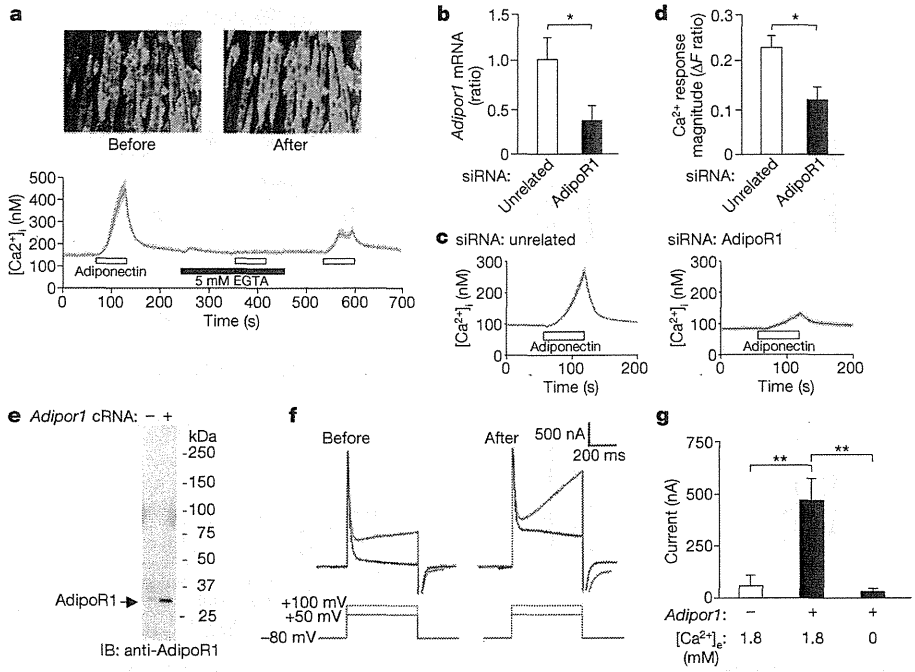

Figure 4 | Adiponectin-induced Ca^{2+} influx by AdipoR1 in C2C12 myocytes and *Xenopus* oocytes. **a**, Pseudocoloured images of changes in fura-2 before and after 1 min stimulation with adiponectin (30 μg ml^{-1}). Red corresponds to the greatest response. The bottom trace demonstrates the average calcium response of C2C12 myocytes to 1-min stimulation with adiponectin along with application of 5 mM EGTA (black bar). The shaded region around the trace represents s.e.m. **b–d**, *Adipor1* mRNA levels (**b**), fura-2 calcium response (**c**) and their magnitude (**d**) of C2C12 myocytes transfected with unrelated siRNA duplex or AdipoR1 siRNA duplex to stimulation with 30 μg ml^{-1} adiponectin for 1 min. **e–g**, The amounts of AdipoR1 protein (**e**), representative Ca^{2+}-activated Cl^- current traces (**f**) before (left) and after (right) 30-s application of adiponectin, and their magnitude (**g**) in *Xenopus* oocytes injected with or without *Adipor1* cRNA in response to adiponectin (30 μg ml^{-1}), and with or without application of 5 mM EGTA with depolarizing pulses of +100 mV. $[Ca^{2+}]_i$ and $[Ca^{2+}]_e$, intracellular and external Ca^{2+} concentration, respectively. All values are presented as mean ± s.e.m. $n = 6$–14, $^*P < 0.05$ and $^{**}P < 0.01$ compared to unrelated siRNA cells or control cells or as indicated.

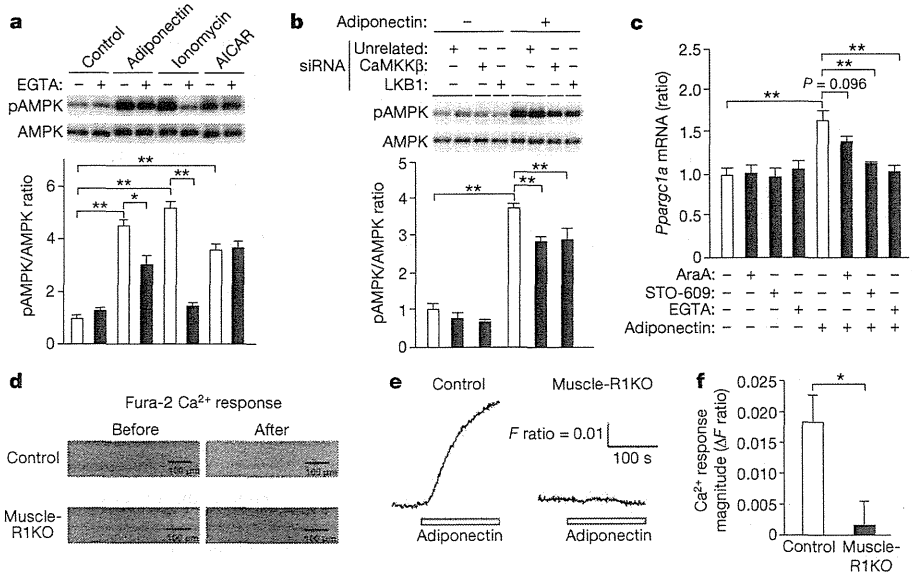

Figure 5 | Adiponectin-induced Ca^{2+} influx is required for CaMKK and AMPK activation and PGC-1α expression. **a**, **b**, Phosphorylation and amount of AMPK in C2C12 myocytes preincubated for 20 min with or without 5 mM EGTA and then treated for 5 min with adiponectin (30 μg ml^{-1}) or ionomycin (1 μM), or for 1 h with AICAR (1 mM) (**a**), or C2C12 myocytes transfected with the indicated siRNA duplex and then treated with 30 μg ml^{-1} adiponectin for 5 min (**b**). **c**, Amount of *Ppargc1a* mRNA in C2C12 myocytes preincubated for 1 h with AraA (0.5 mM) or for 6 h with STO-609 (1 μg ml^{-1}) or for 20 min with EGTA (5 mM), and then treated for 1.5 h with or without adiponectin (10 μg ml^{-1}). **d**, Representative pseudocoloured images of changes in the fura-2 calcium response before and after 5 min stimulation with adiponectin (30 μg ml^{-1}) in a soleus muscle from control mice (top) and muscle-R1KO mice (bottom). Red corresponds to the greatest response. Scale bars, 100 μm. **e**, Trace demonstrates the calcium response of soleus muscle in the fields presented in **d**. Adiponectin was applied during the indicated period. **f**, The magnitude of fura-2 calcium response signals by 160-s adiponectin stimulation to soleus muscles. Δ*F* ratio indicates the change in the fluorescence ratio after adiponectin application. All values are presented as mean ± s.e.m. $n = 5$–10, $^*P < 0.05$ and $^{**}P < 0.01$ compared to control or unrelated siRNA cells or as indicated.

©2010 Macmillan Publishers Limited. All rights reserved